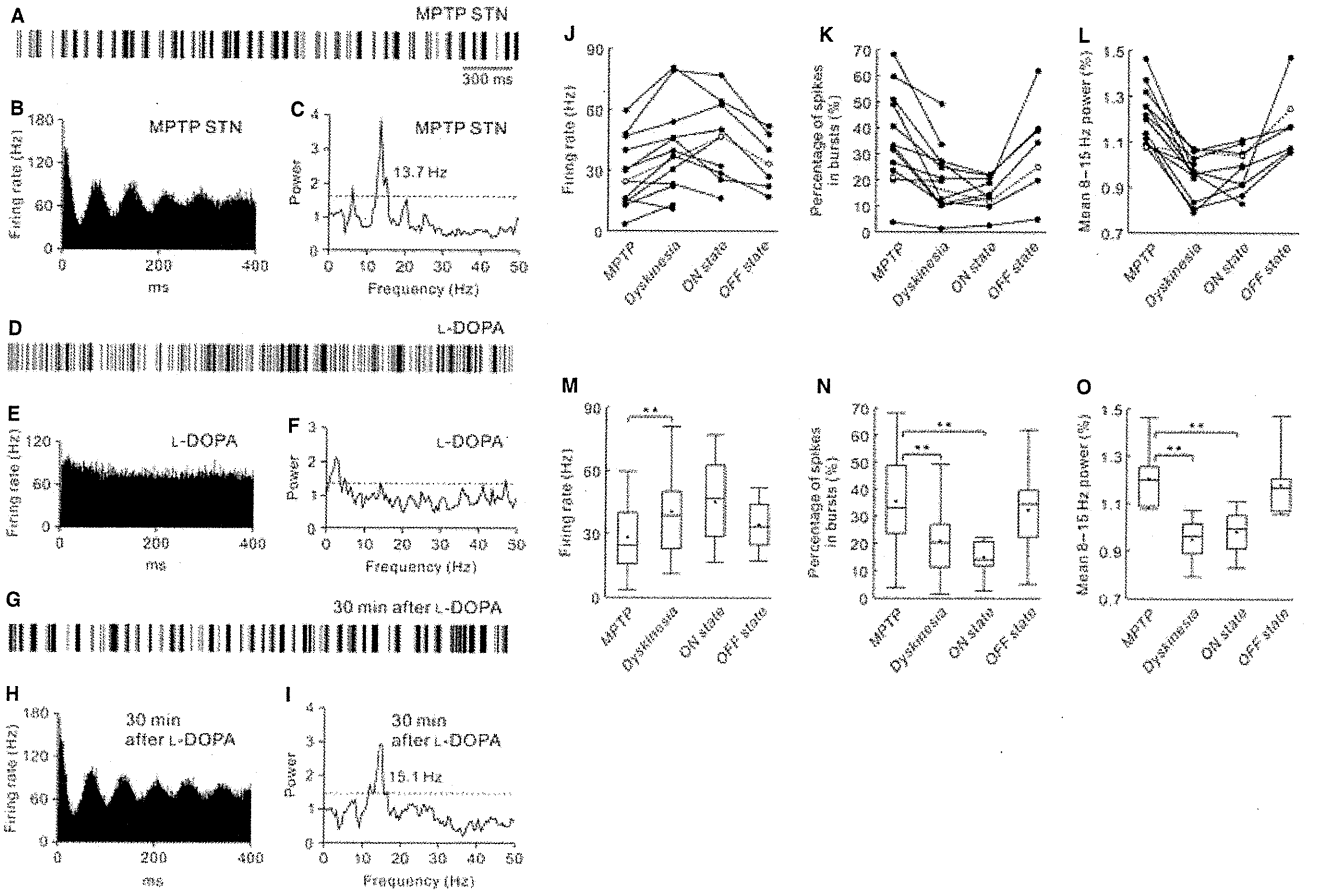

FIG. 7. L-DOPA effects on dopamine-depleted STN neurons. (A–C) An STN neuron showed oscillations in the parkinsonian state. (D–F) An intravenous L-DOPA injection increased the firing rate and suppressed the 8–15-Hz oscillatory activity of the STN neuron during the ON state. In this example, 3–8-Hz oscillations were also attenuated. (G–I) Thirty minutes after the L-DOPA injection, the oscillatory activity appeared again. (J–L) L-DOPA-induced changes in the spontaneous firing rate (J), the burst strength (K) and the mean 8–15-Hz power (L) of 13 STN neurons tested. Data from the neuron recorded without dyskinesia (open circles and broken lines) are superimposed on those from the neurons recorded with dyskinesia (filled circles and solid lines). (M–O) Summaries of the L-DOPA effects on the firing rate (M), the burst strength (N) and the mean 8–15-Hz power (O) in the STN neurons. The average firing rate was increased from pre-injection states to dyskinetic states. On the other hand, there were significant decreases in the burst strength and the mean power of 8–15-Hz oscillations from pre-injection states to dyskinetic states and to ON states. $^{**}P < 0.01$.

electrode for 30 s. The monkeys were deeply anesthetized with intravenous sodium pentobarbital (50 mg/kg) and perfused transcardially with the same methods as reported previously (Kaneda *et al.*, 2005). Serial 60-μm sections were processed for Nissl staining or tyrosine hydroxylase (TH) immunostaining by the same methods as described elsewhere (Kaneda *et al.*, 2005; Tachibana *et al.*, 2008). The recording and drug injection sites were confirmed according to the lesions made by the cathodal DC current and the traces of electrode tracks.

Statistical analysis

All of the data are represented as mean ± SD. Statistical tests were performed with SPSS (IBM, Armonk, NY, USA). Because we made an effort to minimize the damage to brain tissues caused by drug injections, the sample size was not large throughout the experiments. Therefore, we performed a non-parametric Wilcoxon signed-rank test or Mann–Whitney *U*-test for all neuronal data sets. The proportions of oscillatory cells in normal and parkinsonian states were compared by the use of Fisher's exact test. Significance levels were generally set as $P = 0.05$. In the studies with L-DOPA injections, however, we set the significant levels at $P = 0.01$, because the Wilcoxon signed-rank tests were repeatedly performed.

Results

Behavioral and neuronal changes after MPTP injections

We produced the primate model of PD via a unilateral MPTP injection into the internal carotid artery and additional intravenous injections of MPTP. TH immunohistochemistry confirmed the loss of dopaminergic terminals in the putamen and dopaminergic neurons in the substantia nigra of the two MPTP-treated monkeys that served as subjects in this study (Fig. 2A and B). The reduction in TH immunoreactivity was more prominent in the ventral and lateral portions than in the dorsal and medial portions of the substantia nigra of MPTP-treated monkeys; selective loss of dopaminergic neurons by MPTP induction is commonly observed in human PD patients (Yamada *et al.*, 1990; Kaneda *et al.*, 2003). Both monkeys showed obvious parkinsonian signs, such as akinesia/bradykinesia, rigidity, and flexed posture, more severely on the side of the body contralateral to the carotid artery MPTP injection (Fig. 3A). Monkey

parkinsonian scores (Smith *et al.*, 1993; see also Supporting Information Data S1) of the contralateral side to the carotid injections were 11–12 in monkey K (contralateral side: tremor, 0–1/3; posture, 1/2; gait, 3/4; bradykinesia, 3/4; balance, 1/2; gross motor skill, 2/3; defense reaction, 1/2) (ipsilateral side: tremor, 0/3; bradykinesia, 3/4; gross motor skill, 2/3) and 13–14 in monkey Q (contralateral side: tremor, 0/3; posture, 2/2; gait, 3–4/4; bradykinesia, 3/4; balance, 1/2; gross motor skill, 3/3; defense reaction, 1/2) (ipsilateral side: tremor, 0/3; bradykinesia, 3/4; gross motor skill, 2/3). Monkey K occasionally showed weak limb tremor, with peak frequencies of 7.8 and 12.7 Hz (Fig. 3B) (see also Heimer *et al.*, 2006), whereas monkey Q showed no visible tremor. The parkinsonian scores were stable throughout the recording sessions.

Figure 4 and Table 1 show the electrophysiological properties of BG neurons in the normal and parkinsonian states. As compared with the normal state, the average firing rates of GPe and STN neurons in the parkinsonian state were significantly decreased and increased, respectively. However, no changes were detected in the firing rate of GPi neurons. Burst strength was increased from the normal to the parkinsonian state in the GPe, GPi, and STN. Both parkinsonian monkeys showed increases in the number of neurons that oscillated in the 8–15-Hz range in all three of the structures, whereas there were no consistent changes in the number of 3–8-Hz oscillatory cells. The mean power of the 8–15-Hz oscillations increased in all of the structures. Indeed, neurons in the GPi and STN of the two parkinsonian monkeys displayed remarkable tendencies to produce oscillatory bursts, as shown by rhythmic spike trains, and multiple peaks in the autocorrelograms, and power spectrum (e.g. Figs 5A–C and 7A–C). Although the power of 8–15-Hz oscillations in the GPe tended to be weaker than those in the GPi and STN, the oscillatory bursts were also observed in GPe neurons (Fig. 6). The peak frequency with a maximum power of the oscillatory bursts was approximately 13 Hz in all three structures in both monkeys. We also analyzed the power of 20–30-Hz oscillatory activity in the BG, but we did not find a significant increase from normal to parkinsonian conditions (monkey K, GPe, 0.87 ± 0.08 to 0.87 ± 0.15; monkey K, GPi, 0.86 ± 0.12 to 0.77 ± 0.14; monkey K, STN, 0.95 ± 0.06 to 0.84 ± 0.13; monkey Q, GPe, 0.83 ± 0.18 to 0.79 ± 0.15; monkey Q, GPi, 0.90 ± 0.12 to 0.81 ± 0.16; monkey Q, STN, 0.96 ± 0.08 to 0.84 ± 0.13; mean ± SD). Thus, for the following drug injection studies, we pooled the neuronal data from two monkeys and focused on the 8–15-Hz oscillations.

Dopamine dependence of 8–15-Hz oscillations in the BG

We examined the effects of systemic dopamine administration on the neuronal activity of GPi/GPe and STN neurons under parkinsonian conditions (Fig. 1A). Across the L-DOPA injections tested, the behavioral effects appeared within 5 min, and parkinsonian motor scores (such as tremor, bradykinesia, and gross motor skill) were improved by 3–5 (ON state). In more than half of the cases, the animals developed dyskinetic movements in the orofacial and/or forelimb areas prior to the ON state (see Materials and methods). The excessive dyskinetic states usually ceased in 5–10 min. Approximately 30 min after each injection, the animals showed the original parkinsonism (OFF state). In a representative GPi neuron, an intravenous L-DOPA injection decreased the 8–15-Hz oscillations in the ON state (Fig. 5A–F), and the abnormal oscillations appeared again in the OFF state (Fig. 5G–I). In 29 GPi neurons examined, the overall firing rate was not changed throughout the injections (Fig. 5M; Wilcoxon signed-rank test). In contrast, the mean power

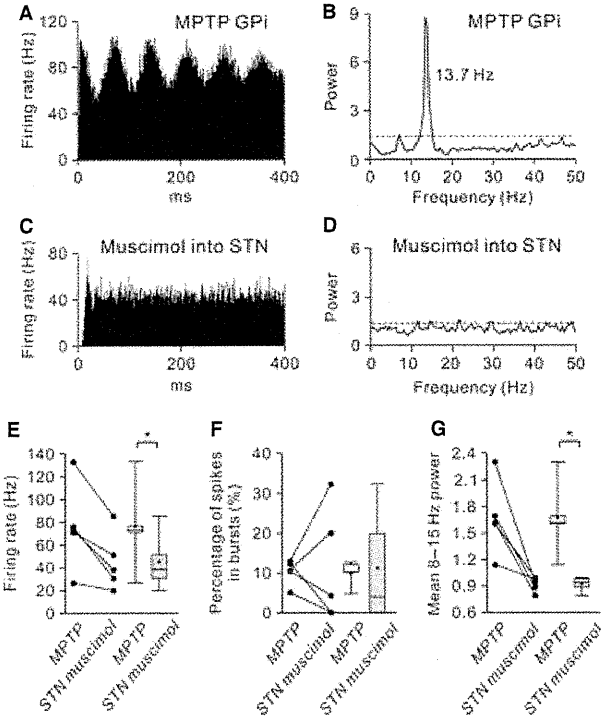

FIG. 8. Effects of STN inactivation on dopamine-depleted GPi neurons. (A and B) A GPi neuron showed abnormal oscillations in the parkinsonian state. (C and D) Muscimol inactivation of the STN decreased the firing rate, and suppressed 8–15-Hz oscillatory activity in the GPi. (E–G) Summaries of the effects of muscimol inactivation of the STN on the spontaneous firing rate (E), the burst strength (F) and the mean 8–15-Hz power spectrum of spike trains (G) in five GPi neurons examined. The STN inactivation significantly decreased the firing rate and the 8–15-Hz power of oscillations in the GPi. $*P < 0.05$.

of 8–15-Hz oscillations was significantly decreased from pre-injection states to dyskinetic states (Fig. 5O; $P < 0.001$, Wilcoxon signed-rank test) and to ON states ($P < 0.001$). Significant decreases in the burst strength were also detected between pre-injection states and ON states (Fig. 5N; $P < 0.001$, Wilcoxon signed-rank test). Although there was a tendency for the power of 8–15-Hz oscillations in dyskinetic states to be lower than that in ON states, we did not detect significant differences in the three parameters (i.e. firing rate, burst strength, and 8–15-Hz oscillatory power) between dyskinetic states and ON states. Similarly, the decreases in abnormal oscillatory bursts of GPe neurons were observed after L-DOPA injections, even though the average firing rate did not change across the recorded population (Fig. 6).

L-DOPA administration also suppressed 8–15-Hz oscillations in the STN (Fig. 7A–F). The abnormal oscillations were concomitant with the re-emergence of parkinsonian motor signs (Fig. 7G–I). In contrast to what was found for GPi/GPe neurons, the average firing rate of 13 STN neurons tested was increased from pre-injection states to dyskinetic states (Fig. 7M; $P = 0.005$). On the other hand, significant decreases in the burst strength (Fig. 7N) and the mean power of 8–15-Hz oscillations (Fig. 7O) were observed from pre-injection states to dyskinetic states ($P = 0.002$ for burst strength; $P = 0.002$ for 8–15-Hz oscillatory power) and to ON states ($P = 0.002$ for burst strength; $P = 0.008$ for 8–15-Hz oscillatory power). Thus far, we have demonstrated that abnormal burst firing and 8–15-Hz oscillatory activity in the GPi/GPe and STN are related to dopamine deficiency.

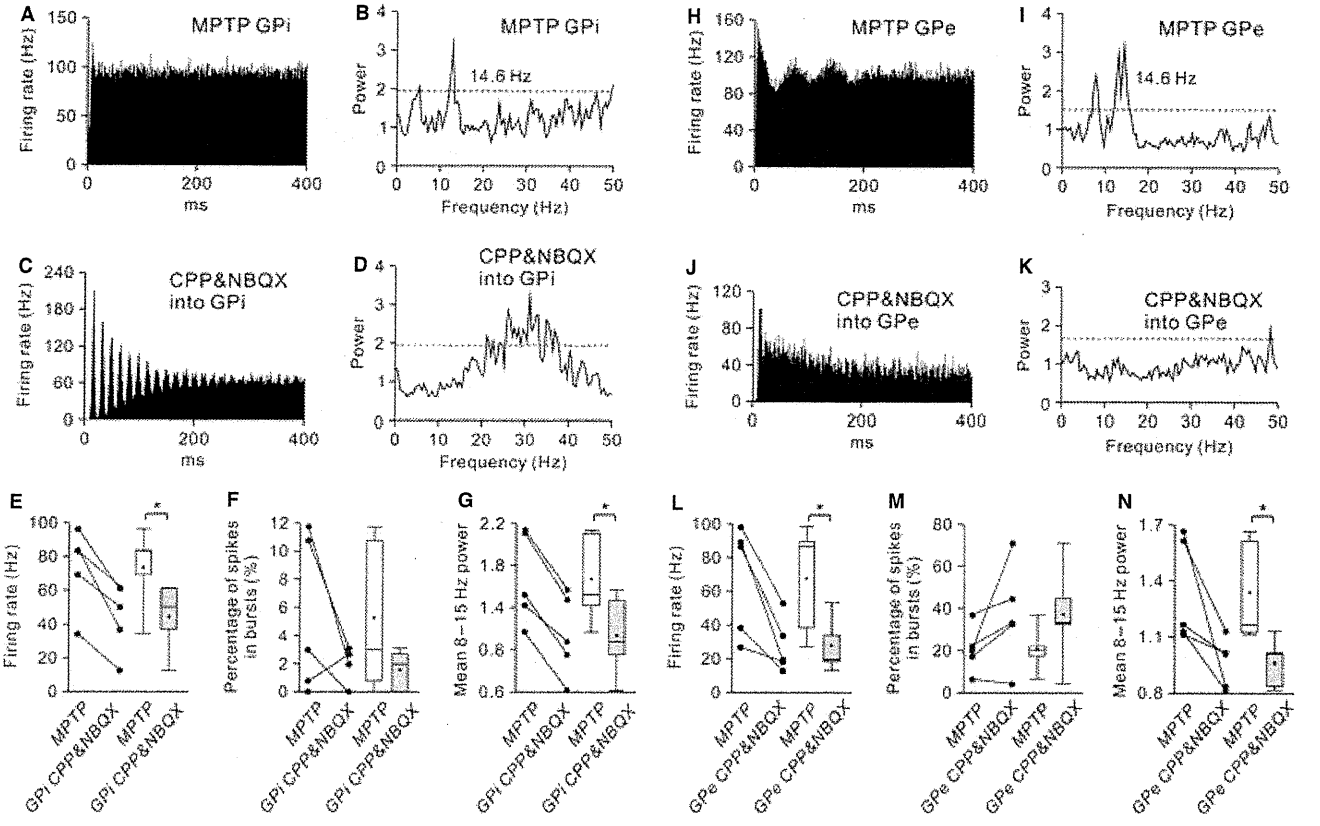

FIG. 9. Effects of intrapallidal blockade of ionotropic glutamatergic neurotransmission on dopamine-depleted GPi/GPe neurons. (A, B, H and I) A pallidal neuron (GPi, A and B; GPe, H and I) showed 3–8-Hz and 8–15-Hz oscillations in the parkinsonian state. (C, D, J and K) Microinjection of a mixture of CPP and NBQX in the vicinity of recorded GPi (C and D) and GPe (J and K) neurons decreased both the firing rates and oscillations. (E–G and L–N) Summaries of the effects of CPP and NBQX microinjections on the spontaneous firing rate (E and L), the burst strength (F and M) and the mean 8–15-Hz power spectrum of spike trains (G and N) in five GPi (E–G) and five GPe (L–N) neurons examined. Injections of CPP and NBQX significantly decreased the firing rate and the 8–15-Hz oscillatory power in the GPi and GPe. $*P < 0.05$.

Origins of abnormal 8–15-Hz oscillations in the GPi/GPe

The GPi and GPe receive glutamatergic inputs from the STN and GABAergic inputs from the striatum and/or GPe. To determine which inputs contribute to abnormal 8–15-Hz oscillations in the GPi, we first performed muscimol inactivation of the STN while simultaneously recording GPi neuronal activity (Fig. 1B). In all five cases, inactivation of the STN ameliorated parkinsonian motor signs, especially bradykinesia and rigidity, as previously reported (Bergman *et al.*, 1990; Wichmann *et al.*, 1994; Levy *et al.*, 2001b). The STN inactivation substantially decreased the 8–15-Hz oscillations (Fig. 8A–D and G; $P = 0.04$) and the firing rate (Fig. 8E; $P = 0.04$) in five GPi neurons, but no consistent changes were detected in the burst strength (Fig. 8F; $P = 0.89$). To obtain further evidence for subthalamic impacts on the oscillatory activity in the GPi/GPe, we also examined whether the intrapallidal blockade of ionotropic glutamate receptors could eliminate the GPi/GPe oscillations (Fig. 1C). Microinjection of a mixture of CPP and NBQX in the vicinity of recorded GPi/GPe neurons significantly decreased the average firing rate (Fig. 9A–D, H–K, E and L; $P = 0.04$ for both the GPi and GPe) and 8–15-Hz oscillations (Fig. 9G and N; $P = 0.04$ for both the GPi and GPe) in the GPi and GPe, whereas the burst strength was not changed uniformly in either structure (Fig. 9F and M; $P = 0.14$ for GPi; $P = 0.08$ for GPe).

We further tested whether GABAergic inputs from the striatum and/or GPe could affect the oscillatory activity of GPi/GPe neurons (Fig. 1D). Microinjection of gabazine in the area surrounding recorded GPi/GPe neurons increased the firing rate of all of the neurons tested (Fig. 10A and C; $P = 0.02$ for GPi; $P = 0.04$ for GPe), and augmented the 8–15-Hz oscillations in the GPi (Fig. 10B; $P = 0.04$), but induced no significant changes in GPe oscillations (Fig. 10D; $P = 0.23$). The burst strength was not changed after the injections (GPi, $n = 7$, $P = 0.17$, Wilcoxon signed-rank test; GPe, $n = 5$, $P = 0.14$, Wilcoxon signed-rank test; data not shown). These results suggest that 8–15-Hz oscillations in the GPi/GPe originate from glutamatergic inputs mainly from the STN.

Origins of abnormal 8–15-Hz oscillations in the STN

The STN is known to receive glutamatergic inputs from the cerebral cortex and the thalamus, and GABAergic inputs from the GPe (Kitai & Deniau, 1981; Kita *et al.*, 1983; Bevan *et al.*, 1995). We first tested whether the elimination of ionotropic glutamatergic inputs could affect the generation of abnormal oscillatory activity in the STN (Fig. 1E). Local injections of a mixture of CPP and NBQX in the vicinity of recorded neurons suppressed the 8–15-Hz oscillations (Fig. 11A–D and G; $P = 0.03$), but increased their burst activities (Fig. 11F; $P = 0.03$), in six STN neurons tested. Such local injections did not induce consistent changes in the firing rate (Fig. 11E; $P = 0.84$).

We further examined whether the interruption of GPe-derived GABAergic inputs can suppress oscillations in the STN (Fig. 1F).

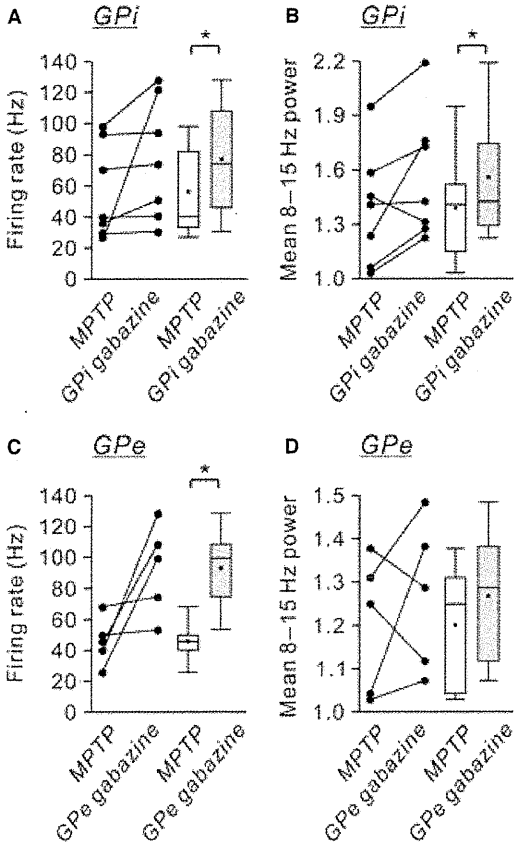

FIG. 10. Effects of intrapallidal blockade of ionotropic GABAergic neurotransmission on dopamine-depleted GPi/GPe neurons. Effects of intrapallidal gabazine microinjections on the spontaneous firing rate (A and C) and the mean 8–15-Hz power spectrum of spike trains (B and D) in seven GPi (A and B) and five GPe (C and D) neurons examined in the parkinsonian state. Injections of gabazine significantly increased the firing rates of GPi/GPe neurons, and increased the 8–15-Hz oscillatory power in the GPi. $*P < 0.05$.

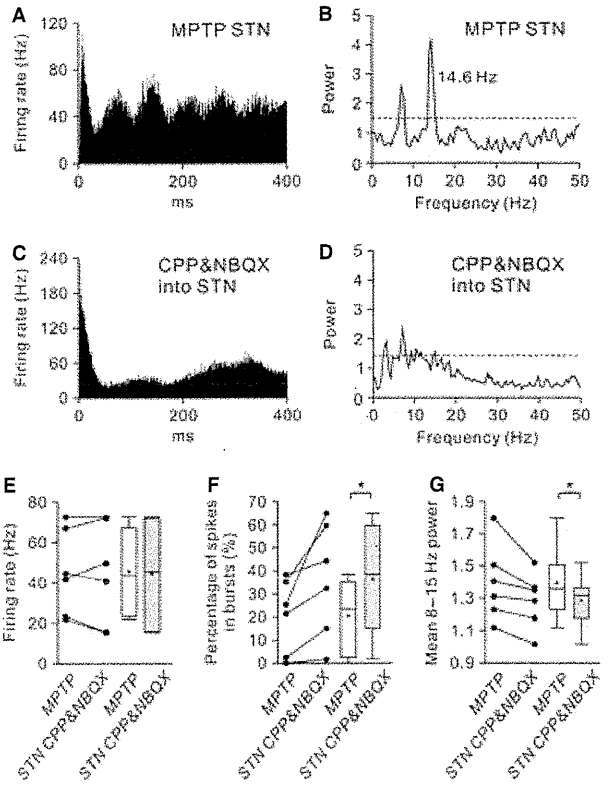

FIG. 11. Effects of intrasubthalamic blockade of ionotropic glutamatergic neurotransmission on dopamine-depleted STN neurons. (A and B) An STN neuron showed abnormal oscillatory bursts in the parkinsonian state. (C and D) Intrasubthalamic microinjection of a mixture of CPP and NBQX decreased 3–8-Hz and 8–15-Hz oscillations in the STN. On the other hand, the injection increased burst firing of the neuron. (E–G) Summaries of the effects of intrasubthalamic microinjections of CPP and NBQX on the spontaneous firing rate (E), the burst strength (F) and the mean 8–15-Hz power spectrum of spike trains (G) in six STN neurons examined. The microinjections of CPP and NBQX significantly decreased the 8–15-Hz oscillatory power, but increased the burst strength in the STN. $*P < 0.05$.

Muscimol inactivation of the GPe attenuated the 8–15-Hz oscillations (Fig. 12A–D and G; $P = 0.03$) and the burst strength (Fig. 12F; $P = 0.03$), and increased the firing rate (Fig. 12E; $P = 0.03$), in six STN neurons tested. In contrast to muscimol inactivation of the STN, the GPe inactivation induced no clear behavioral changes. Taking these findings together, we conclude that the STN oscillatory rhythm is generated by both glutamatergic and GABAergic inputs to the STN.

Discussion

Our results show that loss of nigral dopamine neurons induced abnormal oscillations of GPi/GPe and STN neurons. The GPi/GPe and STN oscillations were reversed by systemic dopamine administration. Notably, direct manipulations of synaptic transmission within the BG of awake parkinsonian primates showed that STN oscillations induced oscillatory activity in the 8–15-Hz range in the GPi/GPe. We further demonstrated that the STN oscillations were strongly driven by (i) glutamatergic inputs, which are thought to arise mainly from the cortex, and (ii) GABAergic inputs from the GPe. These findings suggest that, in the dopamine-depleted state, glutamatergic inputs to the STN and reciprocal GPe–STN interconnections are both important for the generation and amplification of the oscillatory activity of STN neurons, which is subsequently transmitted to the GPi (Fig. 13).

The classic model of PD pathophysiology suggests that degeneration of dopaminergic neurons leads to suppression of the striato-GPi 'direct' pathway and enhancement of the striato-GPe 'indirect' pathway; the increased GPi outputs attenuate thalamocortical neuron activity and induce parkinsonian motor signs (Albin *et al.*, 1989; DeLong, 1990). In this study, two MPTP-treated monkeys exhibited significant firing rate changes in STN neurons, but not in GPi neurons. Several reviews have emphasized that parkinsonism is directly related to BG oscillations (Boraud *et al.*, 2002; Brown, 2003; Gatev *et al.*, 2006; Rivlin-Etzion *et al.*, 2006a; Hammond *et al.*, 2007). The first goal of the present study was to test whether the abnormal BG oscillations depend on dopaminergic inputs. We confirmed that abnormal 8–15-Hz oscillations were increased in the GPi/GPe and STN of dopamine-depleted monkey brain, and were reversed after intravenous L-DOPA injections, with improvements in parkinsonian signs (Heimer *et al.*, 2006). Contrary to expectations, the firing rate of STN neurons increased following the L-DOPA injections. As in the striatum, L-DOPA might be converted to dopamine, which could be released from axon terminals of the remaining dopaminergic and serotonergic neurons in the STN (Lavoie & Parent, 1990; Francois *et al.*, 2000; Bezard *et al.*, 2001). Thus, L-DOPA could increase the firing rate of monkey

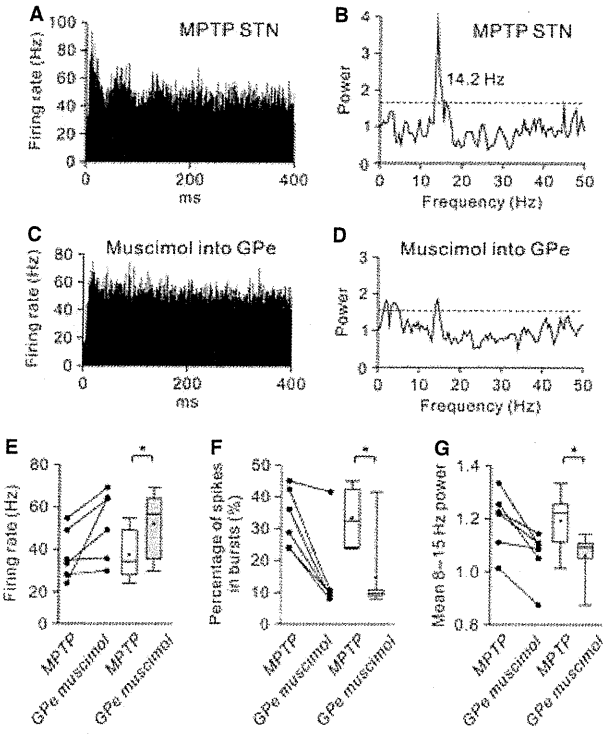

FIG. 12. Effects of GPe inactivation on dopamine-depleted STN neurons. (A and B) An STN neuron showed abnormal 8–15-Hz oscillations in the parkinsonian state. (C and D) Muscimol inactivation of the GPe decreased the 8–15-Hz oscillations in the STN, with an increase in the firing rate. (E–G) Summaries of the effects of muscimol inactivation of the GPe on the spontaneous firing rate (E), the burst strength (F) and the mean 8–15-Hz power spectrum of spike trains (G) in six STN neurons examined. Across the recorded population, the burst strength and the 8–15-Hz oscillations in the STN were decreased after GPe inactivation, whereas the GPe inactivation increased the firing rates of STN neurons. $^*P < 0.05$.

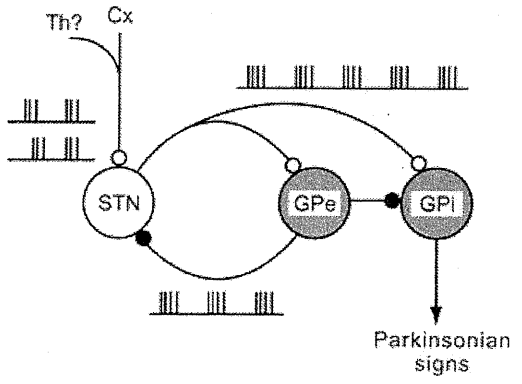

FIG. 13. Schematic diagram showing neural circuits involved in the generation of BG oscillations. In the dopamine-depleted state, a cooperative action of glutamatergic inputs from the cortex (Cx) [and perhaps also from the thalamus (Th)] and reciprocal GPe–STN interconnections can generate and amplify the oscillatory activity of STN neurons. The STN oscillations are finally transmitted to the GPi, thus contributing to the expression of parkinsonian motor signs. Open and filled circles represent glutamatergic and GABAergic synapses, respectively.

STN neurons by eliciting the presynaptic suppression of GABAergic inputs via the direct activation of D2-like receptors (Shen & Johnson, 2000, 2005; Baufreton & Bevan, 2008).

We may predict that L-DOPA injections could reverse the decrease in the GPe firing rate after MPTP treatment. In contrast to previous reports that L-DOPA injections reversed the decrease in the rate of GPe neuron firing after MPTP treatment (Boraud *et al.*, 1998; Heimer *et al.*, 2006), we could not detect such a change uniformly. Increased STN activity may excite some GPe neurons, which may then inhibit other neighboring GPe neurons through GPe–GPe intranuclear axon collaterals (Kita & Kitai, 1994; Nambu & Llinás, 1997; Sato *et al.*, 2000). The data obtained from our L-DOPA studies suggest that normalization of neuronal oscillations in the GPi/GPe and STN may be more critical for L-DOPA actions in parkinsonian signs than changes in their spontaneous firing rates.

Our next aim was to determine the origin of 8–15-Hz oscillations of GPi/GPe neurons. The GPi/GPe receives glutamatergic inputs mainly from the STN and striatal GABAergic inputs (for review, see Smith *et al.*, 1998). The GPi/GPe also receives GABAergic inputs from the GPe through the GPe–GPi projection and the intranuclear collaterals (Hazrati *et al.*, 1990). However, no studies have demonstrated coherent activity between striatal projection neurons and GPi/GPe neurons. Here, we hypothesized that the GPi/GPe oscillations may be generated by glutamatergic inputs from the STN. Our findings revealed that STN inactivation simultaneously decreased the firing rate of GPi neurons, dampened their 8–15-Hz oscillations, and improved parkinsonian motor signs (see also Wichmann *et al.*, 1994). Moreover, microinjection of ionotropic glutamate receptor antagonists reduced the spontaneous firing rate and oscillatory activity in GPi/GPe neurons. In contrast, the 8–15-Hz oscillations were exaggerated or unchanged after microinjection of an ionotropic GABA receptor antagonist. These data suggest that the oscillatory events of GPi/GPe neurons are generated by glutamatergic inputs mainly from the STN, but not by GABAergic inputs from the striatum and GPe.

The final objective of this study was to elucidate the origin of 8–15-Hz oscillations in the STN. The glutamatergic afferents of the STN, which originate from the cortex and the thalamus, constitute one possibility (Kitai & Deniau, 1981; Bevan *et al.*, 1995). The present data showed that the STN oscillations were suppressed after the intrasubthalamic microinjection of ionotropic glutamate receptor antagonists. This suggests that the STN oscillations are partly formed by glutamatergic inputs to the STN. In accordance with the present result, estimates of coherence between the electrocorticogram and the STN LFPs/STN unit activity in the parkinsonian state have suggested that cortical glutamatergic inputs can drive STN oscillations in frequency bands below 30 Hz (Magill *et al.*, 2000, 2001; Sharott *et al.*, 2005; Mallet *et al.*, 2008b). The other possible glutamatergic sources of the primate STN are the intralaminar thalamic nuclei (Lanciego *et al.*, 2009). The parafascicular thalamic nucleus (PF) neurons in the rat PD model show some increased oscillatory activity (in the 0.5–2.5-Hz range) as compared with controls, but simultaneous recording of STN and PF neurons indicates that a majority of PF neurons fire after STN firing (Parr-Brownlie *et al.*, 2009). The contribution of thalamosubthalamic glutamatergic afferents to STN oscillations needs to be further elucidated. Another candidate for the origin of STN oscillations comprises the GABAergic inputs from the GPe, which is interconnected with the STN (Baufreton *et al.*, 2005a). A recent *in vivo* rat study has indicated that dopamine depletion develops the 15–30-Hz oscillations between single GPe–STN neuron pairs (Mallet *et al.*, 2008a). We demonstrated that muscimol inactivation of the GPe attenuated the 8–15-Hz oscillatory activity of STN neurons and suppressed their burst firing properties. This result indicates that the GABAergic inputs from the GPe are likely to contribute to the production of the 8–15-Hz oscillatory bursts in the STN. The decrease in dopaminergic innervation of the GPe in MPTP-

treated monkeys (Schneider & Dacko, 1991) can augment the GPe–GPe GABAergic transmission (Watanabe *et al.*, 2009). The glutamatergic inputs with synchronized GABAergic inputs from the GPe may accelerate the rhythmic phase-locked activity in parkinsonian STN neurons, where dopaminergic innervation of the STN is lacking (Shen & Johnson, 2000, 2005; Baufreton *et al.*, 2005b; Baufreton & Bevan, 2008).

The present study focused on the 8–15-Hz oscillations in the BG of parkinsonian monkeys. LFPs recorded from the GPi/GPe and STN of parkinsonian rodents and PD patients exhibit dopamine-dependent synchronization in the higher 15–30-Hz range (Brown *et al.*, 2001; Cassidy *et al.*, 2002; Sharott *et al.*, 2005; Mallet *et al.*, 2008a,b). Single-unit recordings in the STN of PD patients, however, have demonstrated neuronal oscillations in the frequency range of 10–25 Hz (Levy *et al.*, 2000, 2002), similar to those in MPTP-treated monkeys. The discrepancy in peak frequencies among oscillation/synchronization might be attributable to the difference in the recording setup (Levy *et al.*, 2002), the extent to which loss of dopamine (including other catecholamines) progresses, depending on how parkinsonism is induced (Meredith *et al.*, 2008), and the species-specific intrinsic membrane properties of individual BG neurons and/or emergent properties of the cortico-BG circuit. The BG oscillations in the range below 30 Hz may constrain cortical processing via the BG-thalamocortical pathways (Engel & Fries, 2010). On the other hand, Leblois *et al.* (2007) have reported that oscillatory activity of BG neurons appears after the emergence of severe parkinsonian signs, and concluded that a causal relationship between BG oscillations and PD symptoms is unlikely. There is a possibility that the BG oscillations may merely reflect sensory inputs from the periphery in the states of akinesia/bradykinesia, rigidity, and tremor (Baker, 2007). Here, we simply emphasize that the BG oscillations disappeared when parkinsonian signs were alleviated. In fact, therapeutic approaches, such as dopaminergic medication and STN stimulation, and self-generated movements in human patients are known to decrease the cortico-BG synchronization (Brown *et al.*, 2001, 2004; Cassidy *et al.*, 2002; Levy *et al.*, 2002; Williams *et al.*, 2002; Silberstein *et al.*, 2005; Lafreniere-Roula *et al.*, 2010). In a similar manner, the suppression of the 8–15-Hz oscillations in the primate BG might be required to improve parkinsonian motor signs. We should also mention that BG dysfunction is associated with the abnormal 'dynamic' network properties in the dopamine-depleted BG, owing to the imbalance of neuronal processing between the 'enhanced' cortico-STN-GPi hyperdirect pathway and the 'attenuated' cortico-striato-GPi direct pathway. The BG oscillations generated in the hyperdirect pathway are suggested to serve to limit the 'action selection' properties processed in the direct pathway (Leblois *et al.*, 2006). In addition to the present data showing that STN inactivation suppressed the BG oscillations, our recent studies have revealed that cortically evoked inhibition in the GPi, which is induced via the direct pathway and associated with motor execution (Nambu *et al.*, 2000), is attenuated in the parkinsonian state and restored after STN inactivation (Nambu *et al.*, 2005; Kita & Kita, 2011). These findings suggest the importance of suppression of the 'enhanced' hyperdirect pathway in the reversal of parkinsonian motor signs. Our findings may shed light on the pathophysiology of PD and the exact mechanisms of many current therapies, and will help to develop improved treatments for PD patients.

Supporting Information

Additional supporting information may be found in the online version of this article:

Fig. S1. Three examples of burst detection using the 'Poisson surprise' algorithm.

Data S1. Behavioral criteria of the primate parkinsonian rating scale.

Please note: As a service to our authors and readers, this journal provides supporting information supplied by the authors. Such materials are peer-reviewed and may be re-organized for online delivery, but are not copy-edited or typeset by Wiley-Blackwell. Technical support issues arising from supporting information (other than missing files) should be addressed to the authors.

Acknowledgements

This study was supported by Grants-in-Aid for Scientific Research from the Ministry of Education, Culture, Sports, Science and Technology of Japan, the Japan Intractable Diseases Research Foundation and Hori Information Science Promotion Foundation to Y. Tachibana and A. Nambu, and NIH grants (NS-47085 and NS-57236) to H. Kita. We thank S. Yamamoto and I. Monosov for helpful comments and discussion, M. Meitzler for editing the manuscript, A. Ito, K. Miyamoto and M. Imanishi for technical assistance, and H. Toyoda for MRI scans.

Abbreviations

BG, basal ganglia; CPP, 3-(2-carboxypiperazin-4-yl)-propyl-1-phosphonic acid; GPe, external segment of the globus pallidus; GPi, internal segment of the globus pallidus; L-DOPA, L-3,4-dihydroxyphenylalanine; LFP, local field potential; MPTP, 1-methyl-4-phenyl-1,2,3,6-tetrahydropyridine; NBQX, 1,2,3,4-tetrahydro-6-nitro-2,3-dioxo-benzo[*f*]quinoxaline-7-sulfonamide; PD, Parkinson's disease; PF, parafascicular thalamic nucleus; PSD, power spectral density; SD, standard deviation; STN, subthalamic nucleus; TH, tyrosine hydroxylase.

References

Albin, R.L., Young, A.B. & Penney, J.B. (1989) The functional anatomy of basal ganglia disorders. *Trends Neurosci.*, **12**, 366–375.

Baker, S.N. (2007) Oscillatory interactions between sensorimotor cortex and the periphery. *Curr. Opin. Neurobiol.*, **17**, 649–655.

Baufreton, J. & Bevan, M.D. (2008) D2-like dopamine receptor-mediated modulation of activity-dependent plasticity at GABAergic synapses in the subthalamic nucleus. *J. Physiol.*, **586**, 2121–2142.

Baufreton, J., Atherton, J.F., Surmeier, D.J. & Bevan, M.D. (2005a) Enhancement of excitatory synaptic integration by GABAergic inhibition in the subthalamic nucleus. *J. Neurosci.*, **25**, 8505–8517.

Baufreton, J., Zhu, Z.T., Garret, M., Bioulac, B., Johnson, S.W. & Taupignon, A.I. (2005b) Dopamine receptors set the pattern of activity generated in subthalamic neurons. *FASEB J.*, **19**, 1771–1777.

Bergman, H., Wichmann, T. & DeLong, M.R. (1990) Reversal of experimental parkinsonism by lesions of the subthalamic nucleus. *Science*, **249**, 1436–1438.

Bergman, H., Wichmann, T., Karmon, B. & DeLong, M.R. (1994) The primate subthalamic nucleus. II. Neuronal activity in the MPTP model of parkinsonism. *J. Neurophysiol.*, **72**, 507–520.

Bevan, M.D., Francis, C.M. & Bolam, J.P. (1995) The glutamate-enriched cortical and thalamic input to neurons in the subthalamic nucleus of the rat: convergence with GABA-positive terminals. *J. Comp. Neurol.*, **361**, 491–511.

Bezard, E., Brotchie, J.M. & Gross, C.E. (2001) Pathophysiology of levodopa-induced dyskinesia: potential for new therapies. *Nat. Rev. Neurosci.*, **2**, 577–588.

Boraud, T., Bezard, E., Guehl, D., Bioulac, B. & Gross, C. (1998) Effects of L-DOPA on neuronal activity of the globus pallidus externalis (GPe) and globus pallidus internalis (GPi) in the MPTP-treated monkey. *Brain Res.*, **787**, 157–160.

Boraud, T., Bezard, E., Bioulac, B. & Gross, C.E. (2002) From single extracellular unit recording in experimental and human Parkinsonism to the development of a functional concept of the role played by the basal ganglia in motor control. *Prog. Neurobiol.*, **66**, 265–283.

Brown, P. (2003) Oscillatory nature of human basal ganglia activity: relationship to the pathophysiology of Parkinson's disease. *Mov. Disord.*, **18**, 357–363.

Brown, P., Oliviero, A., Mazzone, P., Insola, A., Tonali, P. & Di Lazzaro, V. (2001) Dopamine dependency of oscillations between subthalamic nucleus and pallidum in Parkinson's disease. *J. Neurosci.*, **21**, 1033–1038.

Brown, P., Mazzone, P., Oliviero, A., Altibrandi, M.G., Pilato, F., Tonali, P.A. & Di Lazzaro, V. (2004) Effects of stimulation of the subthalamic area on oscillatory pallidal activity in Parkinson's disease. *Exp. Neurol.*, **188**, 480–490.

Cassidy, M., Mazzone, P., Oliviero, A., Insola, A., Tonali, P., Di Lazzaro, V. & Brown, P. (2002) Movement-related changes in synchronization in the human basal ganglia. *Brain*, **125**, 1235–1246.

DeLong, M.R. (1990) Primate models of movement disorders of basal ganglia origin. *Trends Neurosci.*, **13**, 281–285.

Engel, A.K. & Fries, P. (2010) Beta-band oscillations – signalling the status quo? *Curr. Opin. Neurobiol.*, **20**, 156–165.

Filion, M. (1979) Effects of interruption of the nigrostriatal pathway and of dopaminergic agents on the spontaneous activity of globus pallidus neurons in the awake monkey. *Brain Res.*, **178**, 425–441.

Francois, C., Savy, C., Jan, C., Tande, D., Hirsch, E.C. & Yelnik, J. (2000) Dopaminergic innervation of the subthalamic nucleus in the normal state, in MPTP-treated monkeys, and in Parkinson's disease patients. *J. Comp. Neurol.*, **425**, 121–129.

Gatev, P., Darbin, O. & Wichmann, T. (2006) Oscillations in the basal ganglia under normal conditions and in movement disorders. *Mov. Disord.*, **21**, 1566–1577.

Halliday, D.M., Rosenberg, J.R., Amjad, A.M., Breeze, P., Conway, B.A. & Farmer, S.F. (1995) A framework for the analysis of mixed time series/point process data-theory and application to the study of physiological tremor, single motor unit discharges and electromyograms. *Prog. Biophys. Mol. Biol.*, **64**, 237–278.

Hammond, C., Bergman, H. & Brown, P. (2007) Pathological synchronization in Parkinson's disease: networks, models and treatments. *Trends Neurosci.*, **30**, 357–364.

Hazrati, L.N., Parent, A., Mitchell, S. & Haber, S.N. (1990) Evidence for interconnections between the two segments of the globus pallidus in primates: a PHA-L anterograde tracing study. *Brain Res.*, **533**, 171–175.

Heimer, G., Rivlin-Etzion, M., Bar-Gad, I., Goldberg, J.A., Haber, S.N. & Bergman, H. (2006) Dopamine replacement therapy does not restore the full spectrum of normal pallidal activity in the 1-methyl-4-phenyl-1,2,3,6-tetra-hydropyridine primate model of Parkinsonism. *J. Neurosci.*, **26**, 8101–8114.

Kaneda, K., Imanishi, M., Nambu, A., Shigemoto, R. & Takada, M. (2003) Differential expression patterns of mGluR1α in monkey nigral dopamine neurons. *Neuroreport*, **14**, 947–950.

Kaneda, K., Tachibana, Y., Imanishi, M., Kita, H., Shigemoto, R., Nambu, A. & Takada, M. (2005) Down-regulation of metabotropic glutamate receptor 1α in globus pallidus and substantia nigra of parkinsonian monkeys. *Eur. J. Neurosci.*, **22**, 3241–3254.

Kita, H. & Kita, T. (2011) Cortical stimulation evokes abnormal responses in the dopamine-depleted rat basal ganglia. *J. Neurosci.*, **31**, 10311–10322.

Kita, H. & Kitai, S.T. (1994) The morphology of globus pallidus projection neurons in the rat: an intracellular staining study. *Brain Res.*, **636**, 308–319.

Kita, H., Chang, H.T. & Kitai, S.T. (1983) Pallidal inputs to subthalamus: intracellular analysis. *Brain Res.*, **264**, 255–265.

Kitai, S.T. & Deniau, J.M. (1981) Cortical inputs to the subthalamus: intracellular analysis. *Brain Res.*, **214**, 411–415.

Lafreniere-Roula, M., Darbin, O., Hutchison, W.D., Wichmann, T., Lozano, A.M. & Dostrovsky, J.O. (2010) Apomorphine reduces subthalamic neuronal entropy in parkinsonian patients. *Exp. Neurol.*, **225**, 455–458.

Lanciego, J.L., Lopez, I.P., Rico, A.J., Aymerich, M.S., Perez-Manso, M., Conte, L., Combarro, C., Roda, E., Molina, C., Gonzalo, N., Castle, M., Tunon, T., Erro, E. & Barroso-Chinea, P. (2009) The search for a role of the caudal intralaminar nuclei in the pathophysiology of Parkinson's disease. *Brain Res. Bull.*, **78**, 55–59.

Lavoie, B. & Parent, A. (1990) Immunohistochemical study of the serotoninergic innervation of the basal ganglia in the squirrel monkey. *J. Comp. Neurol.*, **299**, 1–16.

Leblois, A., Boraud, T., Meissner, W., Bergman, H. & Hansel, D. (2006) Competition between feedback loops underlies normal and pathological dynamics in the basal ganglia. *J. Neurosci.*, **26**, 3567–3583.

Leblois, A., Meissner, W., Bioulac, B., Gross, C.E., Hansel, D. & Boraud, T. (2007) Late emergence of synchronized oscillatory activity in the pallidum during progressive Parkinsonism. *Eur. J. Neurosci.*, **26**, 1701–1713.

Levy, R., Hutchison, W.D., Lozano, A.M. & Dostrovsky, J.O. (2000) High-frequency synchronization of neuronal activity in the subthalamic nucleus of parkinsonian patients with limb tremor. *J. Neurosci.*, **20**, 7766–7775.

Levy, R., Dostrovsky, J.O., Lang, A.E., Sime, E., Hutchison, W.D. & Lozano, A.M. (2001a) Effects of apomorphine on subthalamic nucleus and globus pallidus internus neurons in patients with Parkinson's disease. *J. Neurophysiol.*, **86**, 249–260.

Levy, R., Lang, A.E., Dostrovsky, J.O., Pahapill, P., Romas, J., Saint-Cyr, J., Hutchison, W.D. & Lozano, A.M. (2001b) Lidocaine and muscimol microinjections in subthalamic nucleus reverse Parkinsonian symptoms. *Brain*, **124**, 2105–2118.

Levy, R., Ashby, P., Hutchison, W.D., Lang, A.E., Lozano, A.M. & Dostrovsky, J.O. (2002) Dependence of subthalamic nucleus oscillations on movement and dopamine in Parkinson's disease. *Brain*, **125**, 1196–1209.

Magill, P.J., Bolam, J.P. & Bevan, M.D. (2000) Relationship of activity in the subthalamic nucleus–globus pallidus network to cortical electroencephalogram. *J. Neurosci.*, **20**, 820–833.

Magill, P.J., Bolam, J.P. & Bevan, M.D. (2001) Dopamine regulates the impact of the cerebral cortex on the subthalamic nucleus–globus pallidus network. *Neuroscience*, **106**, 313–330.

Mallet, N., Pogosyan, A., Marton, L.F., Bolam, J.P., Brown, P. & Magill, P.J. (2008a) Parkinsonian beta oscillations in the external globus pallidus and their relationship with subthalamic nucleus activity. *J. Neurosci.*, **28**, 14245–14258.

Mallet, N., Pogosyan, A., Sharott, A., Csicsvari, J., Bolam, J.P., Brown, P. & Magill, P.J. (2008b) Disrupted dopamine transmission and the emergence of exaggerated beta oscillations in subthalamic nucleus and cerebral cortex. *J. Neurosci.*, **28**, 4795–4806.

Meredith, G.E., Sonsalla, P.K. & Chesselet, M.F. (2008) Animal models of Parkinson's disease progression. *Acta Neuropathol.*, **115**, 385–398.

Nambu, A. & Llinás, R. (1997) Morphology of globus pallidus neurons: its correlation with electrophysiology in guinea pig brain slices. *J. Comp. Neurol.*, **377**, 85–94.

Nambu, A., Tokuno, H., Hamada, I., Kita, H., Imanishi, M., Akazawa, T., Ikeuchi, Y. & Hasegawa, N. (2000) Excitatory cortical inputs to pallidal neurons via the subthalamic nucleus in the monkey. *J. Neurophysiol.*, **84**, 289–300.

Nambu, A., Tachibana, Y., Kaneda, K., Tokuno, H. & Takada, M. (2005) Dynamic model of basal ganglia functions and parkinson's disease. In Bolam, J.P., Ingham, C.A. & Magill, P.J. (Eds), *The Basal Ganglia VIII*. Springer, New York, pp. 307–312.

Parr-Brownlie, L.C., Poloskey, S.L., Bergstrom, D.A. & Walters, J.R. (2009) Parafascicular thalamic nucleus activity in a rat model of Parkinson's disease. *Exp. Neurol.*, **217**, 269–281.

Priori, A., Foffani, G., Pesenti, A., Tamma, F., Bianchi, A.M., Pellegrini, M., Locatelli, M., Moxon, K.A. & Villani, R.M. (2004) Rhythm-specific pharmacological modulation of subthalamic activity in Parkinson's disease. *Exp. Neurol.*, **189**, 369–379.

Rivlin-Etzion, M., Marmor, O., Heimer, G., Raz, A., Nini, A. & Bergman, H. (2006a) Basal ganglia oscillations and pathophysiology of movement disorders. *Curr. Opin. Neurobiol.*, **16**, 629–637.

Rivlin-Etzion, M., Ritov, Y., Heimer, G., Bergman, H. & Bar-Gad, I. (2006b) Local shuffling of spike trains boosts the accuracy of spike train spectral analysis. *J. Neurophysiol.*, **95**, 3245–3256.

Sato, F., Lavallee, P., Levesque, M. & Parent, A. (2000) Single-axon tracing study of neurons of the external segment of the globus pallidus in primate. *J. Comp. Neurol.*, **417**, 17–31.

Schneider, J.S. & Dacko, S. (1991) Relative sparing of the dopaminergic innervation of the globus pallidus in monkeys made hemi-parkinsonian by intracarotid MPTP infusion. *Brain Res.*, **556**, 292–296.

Sharott, A., Magill, P.J., Harnack, D., Kupsch, A., Meissner, W. & Brown, P. (2005) Dopamine depletion increases the power and coherence of beta-oscillations in the cerebral cortex and subthalamic nucleus of the awake rat. *Eur. J. Neurosci.*, **21**, 1413–1422.

Shen, K.Z. & Johnson, S.W. (2000) Presynaptic dopamine D2 and muscarine M3 receptors inhibit excitatory and inhibitory transmission to rat subthalamic neurones *in vitro*. *J. Physiol.*, **525**(Pt 2), 331–341.

Shen, K.Z. & Johnson, S.W. (2005) Dopamine depletion alters responses to glutamate and GABA in the rat subthalamic nucleus. *Neuroreport*, **16**, 171–174.

Silberstein, P., Pogosyan, A., Kuhn, A.A., Hotton, G., Tisch, S., Kupsch, A., Dowsey-Limousin, P., Hariz, M.I. & Brown, P. (2005) Cortico-cortical coupling in Parkinson's disease and its modulation by therapy. *Brain*, **128**, 1277–1291.

Smith, R.D., Zhang, Z., Kurlan, R., McDermott, M. & Gash, D.M. (1993) Developing a stable bilateral model of parkinsonism in rhesus monkeys. *Neuroscience*, **52**, 7–16.

Smith, Y., Bevan, M.D., Shink, E. & Bolam, J.P. (1998) Microcircuitry of the direct and indirect pathways of the basal ganglia. *Neuroscience*, **86**, 353–387.

Soares, J., Kliem, M.A., Betarbet, R., Greenamyre, J.T., Yamamoto, B. & Wichmann, T. (2004) Role of external pallidal segment in primate parkinsonism: comparison of the effects of 1-methyl-4-phenyl-1,2,3,6-tetrahydropyridine-induced parkinsonism and lesions of the external pallidal segment. *J. Neurosci.*, **24**, 6417–6426.

Tachibana, Y., Kita, H., Chiken, S., Takada, M. & Nambu, A. (2008) Motor cortical control of internal pallidal activity through glutamatergic and GABAergic inputs in awake monkeys. *Eur. J. Neurosci.*, **27**, 238–253.

Watanabe, K., Kita, T. & Kita, H. (2009) Presynaptic actions of D2-like receptors in the rat cortico-striato-globus pallidus disynaptic connection *in vitro*. *J. Neurophysiol.*, **101**, 665–671.

Wichmann, T. & Soares, J. (2006) Neuronal firing before and after burst discharges in the monkey basal ganglia is predictably patterned in the normal state and altered in parkinsonism. *J. Neurophysiol.*, **95**, 2120–2133.

Wichmann, T., Bergman, H. & DeLong, M.R. (1994) The primate subthalamic nucleus. III. Changes in motor behavior and neuronal activity in the internal pallidum induced by subthalamic inactivation in the MPTP model of parkinsonism. *J. Neurophysiol.*, **72**, 521–530.

Williams, D., Tijssen, M., Van Bruggen, G., Bosch, A., Insola, A., Di Lazzaro, V., Mazzone, P., Oliviero, A., Quartarone, A., Speelman, H. & Brown, P. (2002) Dopamine-dependent changes in the functional connectivity between basal ganglia and cerebral cortex in humans. *Brain*, **125**, 1558–1569.

Yamada, T., McGeer, P.L., Baimbridge, K.G. & McGeer, E.G. (1990) Relative sparing in Parkinson's disease of substantia nigra dopamine neurons containing calbindin-D28K. *Brain Res.*, **526**, 303–307.

J Neurophysiol 106: 1203–1217, 2011.
First published June 8, 2011; doi:10.1152/jn.00768.2010.

Differential activity patterns of putaminal neurons with inputs from the primary motor cortex and supplementary motor area in behaving monkeys

Sayuki Takara,[1] Nobuhiko Hatanaka,[1] Masahiko Takada,[2,3] and Atsushi Nambu[1]

[1]*Division of System Neurophysiology, National Institute for Physiological Sciences and Department of Physiological Sciences, The Graduate University for Advanced Studies, Okazaki, Aichi, Japan;* [2]*Department of System Neuroscience, Tokyo Metropolitan Institute for Neuroscience, Fuchu, Tokyo, Japan; and* [3]*Systems Neuroscience Section, Primate Research Institute, Kyoto University, Inuyama, Aichi, Japan*

Submitted 8 September 2010; accepted in final form 4 June 2011

Takara S, Hatanaka N, Takada M, Nambu A. Differential activity patterns of putaminal neurons with inputs from the primary motor cortex and supplementary motor area in behaving monkeys. *J Neurophysiol* 106: 1203–1217, 2011. First published June 8, 2011; doi:10.1152/jn.00768.2010.—Activity patterns of projection neurons in the putamen were investigated in behaving monkeys. Stimulating electrodes were implanted chronically into the proximal ($MI_{proximal}$) and distal (MI_{distal}) forelimb regions of the primary motor cortex (MI) and the forelimb region of the supplementary motor area (SMA). Cortical inputs to putaminal neurons were identified by excitatory orthodromic responses to stimulation of these motor cortices. Then, neuronal activity was recorded during the performance of a goal-directed reaching task with delay. Putaminal neurons with inputs from the MI and SMA showed different activity patterns, i.e., movement- and delay-related activity, during task performance. MI-recipient neurons increased activity in response to arm-reach movements, whereas SMA-recipient neurons increased activity during delay periods, as well as during movements. The activity pattern of MI + SMA-recipient neurons was of an intermediate type between those of MI- and SMA-recipient neurons. Approximately one-half of $MI_{proximal}$-, SMA-, and MI + SMA-recipient neurons changed activities before the onset of movements, whereas a smaller number of MI_{distal}- and $MI_{proximal\ +\ distal}$-recipient neurons did. Movement-related activity of MI-recipient neurons was modulated by target directions, whereas SMA- and MI + SMA-recipient neurons had a lower directional selectivity. MI-recipient neurons were located mainly in the ventrolateral part of the caudal aspect of the putamen, whereas SMA-recipient neurons were located in the dorsomedial part. MI + SMA-recipient neurons were found in between. The present results suggest that a subpopulation of putaminal neurons displays specific activity patterns depending on motor cortical inputs. Each subpopulation receives convergent or nonconvergent inputs from the MI and SMA, retains specific motor information, and sends it to the globus pallidus and the substantia nigra through the direct and indirect pathways of the basal ganglia.

basal ganglia; striatum; motor control; single-unit recording

THE PRIMATE STRIATUM, composed of the putamen, the caudate nucleus, and the ventral striatum, is a main input station of the basal ganglia and receives neural signals from wide areas of the cerebral cortex. Every single striatal projection neuron is estimated to receive diverse inputs from ~750 to 7,500 cortical neurons (Bennet and Wilson 2000), and thus cortical information is massively integrated within the striatum. The activity of striatal projection neurons is strongly modulated by local interneurons that also receive cortical inputs (Tepper et al. 2008). The projection neurons finally send processed signals to the external and internal segments of the globus pallidus and the substantia nigra pars reticulata through the direct and indirect pathways of the basal ganglia. Therefore, to understand the functional roles of striatal projection neurons, it is essential to examine how information from various cortical areas is integrated and represented within the striatum.

Previous electrophysiological studies revealed that the patterns of neural activity differed among subregions of the putamen (Alexander and Crutcher 1990; Kimura et al. 1992; Lee and Assad 2003; Liles 1983; Schultz and Romo 1992). Neurons in the lateral part of the putamen increased activity simply in relation to movements, whereas those in the medial part showed complex activity changes, such as responses to visual stimuli. These different response patterns may reflect difference in cortical inputs. Actually, the forelimb region of the primary motor cortex (MI) projects mainly to the ventrolateral part of the caudal aspect of the putamen, and that of the supplementary motor area (SMA) projects predominantly to the dorsomedial part (Nambu et al. 2002; Takada et al. 1998a, b). The mediolateral central region of the putamen receives convergent inputs from both the MI and SMA. Thus the information about the forelimb movements from the MI and SMA is processed in a convergent or nonconvergent manner within the putamen. To investigate how such cortical inputs are processed and represented in the putaminal projection neurons, their activity during the performance of a goal-directed reaching task with delay was recorded after identification of cortical inputs by stimulation of the MI and SMA in the present study.

MATERIALS AND METHODS

Behavioral task. Two Japanese monkeys of either sex (*Macaca fuscata*; named S and A), weighing 5.2 and 8.0 kg, were used in this experiment. Both monkeys were right-handed. The experimental protocols were approved by the Institutional Animal Care and Use Committee of National Institutes of Natural Sciences, and all experiments were conducted according to the guidelines of the National Institutes of Health *Guide for the Care and Use of Laboratory Animals*.

Each animal was seated in a primate chair and trained to perform a goal-directed reaching task with delay (Fig. 1*A*). Three slots (Left, Center, and Right) were aligned horizontally in a panel that was placed at a distance of 30 cm in front of the animals. Three slots were separated from each other by 10 cm. Each slot was 18 mm in height, 6 mm in width, and 11 mm in depth. A two-color (red and green) light-emitting diode (LED) was installed in the bottom of each slot.

Address for reprint requests and other correspondence: A. Nambu, Division of System Neurophysiology, National Institute for Physiological Sciences, Myodaiji, Okazaki, Aichi 444-8585, Japan (e-mail: nambu@nips.ac.jp).

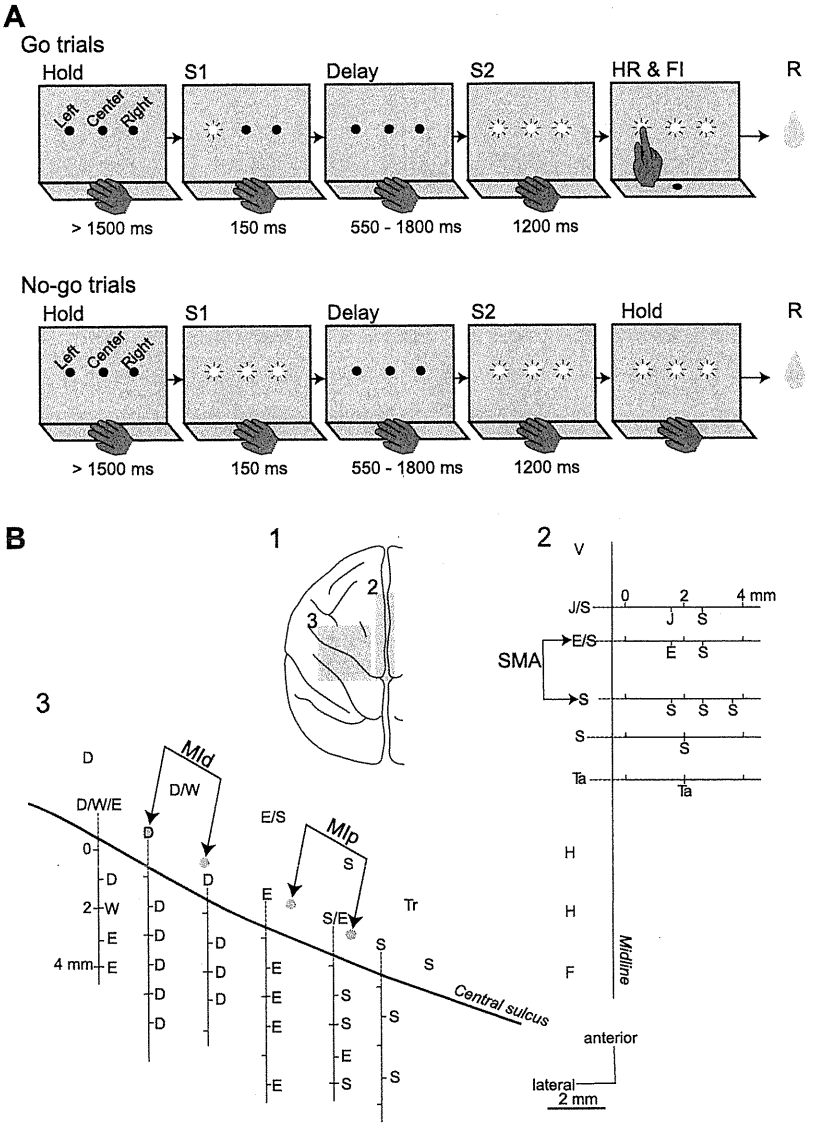

Fig. 1. *A*: goal-directed reaching task with delay. Three slots (Left, Center, and Right) were aligned horizontally in a panel that was placed in front of the animals. A 2-color (red and green) light-emitting diode (LED) was installed in the bottom of each slot. Each trial was initiated after the animal placed its hand at the resting position for at least 1,500 ms. In Go trials, 1 of the 3 LEDs (Left, Center, or Right) was lit with a red color for 150 ms as an instruction stimulus (S1). After a random delay period of 550–1,800 ms, all 3 LEDs were lit with a green color for 1,200 ms as a triggering stimulus (S2). Upon the presentation of the triggering stimulus, the monkey was required to reach out its forelimb and touch, using its index finger, the LED inside the slot that had been instructed previously by the S1. The timings of hand release (HR) from the resting position and of finger in (FI) the slot were detected by the infrared photoelectric sensors. If the monkey touched the correct LED within 1,200 ms, it was rewarded (R) with juice. In No-go trials, all 3 LEDs were lit simultaneously with a red color for 150 ms (S1). After a delay period of 550–1,800 ms, all 3 LEDs were lit with a green color for 1,200 ms (S2). If the monkey kept its hand at the resting position during these periods, it was rewarded with juice. *B*: cortical mapping (Monkey S) for implantation of stimulating electrodes. *B1*: top view of the monkey brain. Gray squares indicate mapped areas in 2 and 3. *B2* and *B3*: mapping of the supplementary motor area (SMA) and primary motor cortex (MI), respectively. Each letter indicates the somatotopic body part: D, digit; E, elbow; F, foot; H, hip; J, jaw; S, shoulder; Ta, tail; Tr, trunk; V, visual response; W, wrist. Somatotopic arrangements in the mesial surface and the rostral bank of the central sulcus are also shown, along with depths from the cortical surface. Three pairs of bipolar-stimulating electrodes were implanted into the loci, indicated by small gray circles: the forearm region of the SMA and the proximal (MIp) and distal (MId) forelimb regions of the MI.

Each trial was initiated after the animal placed its right hand at the resting position that was located below the panel for at least 1,500 ms. In Go trials (Fig. 1*A*), one of three LEDs was lit with a red color for 150 ms as an instruction stimulus. A random delay period of 550–1,800 ms followed the instruction stimulus. During the instruction stimulus and delay period, the monkey was required to keep its hand at the resting position. After a delay period, all three LEDs were lit with a green color for 1,200 ms as a triggering stimulus. Upon the presentation of a triggering stimulus, the monkey was required to reach out its right forelimb, using its index finger, and touch the LED inside the slot that had been directed previously by the instruction stimulus. The onset timings of the instruction stimulus and the triggering stimulus are denoted as S1 and S2, respectively. The timings of hand release (HR) from the resting position and finger in (FI) the slot were detected by infrared photoelectric sensors (Keyence, Osaka, Japan), installed in the resting position and slots. If the monkey touched the correct LED within 1,200 ms, it was rewarded with juice. The onset timing of reward delivery is denoted as R. If the monkey released its hand from the resting position during the instruction stimulus and delay period, touched the wrong LED, or touched the LED after 1,200 ms, it was not rewarded, and the trial with same task conditions was repeated (repeat of the error conditions). In No-go trials (Fig. 1*A*), all three LEDs were lit simultaneously with a red color for 150 ms as an instruction stimulus (S1). After a delay period of 550–1,800 ms, all three LEDs were lit with a green color for 1,200 ms as a triggering stimulus (S2). If the monkey kept its hand at the resting position during the entire delay and triggering-stimulus periods, it was rewarded with juice (R). If the monkey released its hand from the resting position during entire periods, it was not rewarded, and the No-go trial was repeated. Left, Center, and Right targets (appearance probability of each target, 29%) and No-go (13%) trials were presented randomly. Intertrial intervals (between the end of Reward and the beginning of the following trial) were 2,000–3,000 ms.

Surgery. After learning the behavioral task, the monkeys underwent surgical operations to fix their head painlessly in a stereotaxic frame attached to a primate chair (for details, see Nambu et al. 2000, 2002) under general anesthesia with sodium pentobarbital (25 mg/kg body wt, iv) after induction with ketamine hydrochloride (10 mg/kg im) and xylazine hydrochloride (1–2 mg/kg im).

After full recovery from the operation, the skull over the left MI and SMA was removed under light anesthesia with ketamine hydrochloride (10 mg/kg im) and xylazine hydrochloride (1–2 mg/kg im).

The forelimb regions of the MI and SMA were identified by electrophysiological methods (Fig. 1*B*; for details, see Nambu et al. 2000, 2002). According to this mapping, three pairs of bipolar-stimulating electrodes (made of 200 μm-diameter, enamel-coated, stainless-steel wires; intertip distance, 2 mm) were implanted chronically into the MI and SMA: one into the distal forelimb region of the MI (MI_{distal}), another into the proximal forelimb region of the MI ($MI_{proximal}$), and the other into the forelimb region of the SMA. Exposed areas were covered with transparent acrylic resin, except for the orofacial area of the MI (10–15 mm diameter), for access to the putamen. A rectangular plastic chamber covering the hole was fixed onto the skull with acrylic resin.

Single-unit recording of putaminal neurons. Recording neuronal activity of the left putamen was initiated after full recovery from the surgery and was performed 2 or 3 days/wk. During the experimental sessions, each monkey was seated in the monkey chair with head fixation. A glass-coated Elgiloy alloy microelectrode (0.5–1.5 MΩ at 1 kHz) was inserted obliquely (45° from vertical in the frontal plane) through the dura into the putamen to record neuronal activity using a hydraulic microdrive (Narishige Scientific Instrument Laboratory, Tokyo, Japan). The neuronal activity recorded from the microelectrode was amplified (×10,000), filtered (100–2,000 Hz), and displayed on an oscilloscope. The forelimb region of the putamen can be identified by *1*) responses to sensory stimuli of the forelimb and *2*) orthodromic excitation evoked by MI and SMA stimulation (Nambu et al. 2002). Activity of the putaminal neuron was isolated and converted into digital pulses using a time-amplitude window discriminator. The responses to cortical stimulation (300-μs duration single pulse, strength of <0.6 mA, sometimes up to 0.7 mA, at 0.7 Hz) were observed by constructing peristimulus time histograms (PSTHs; bin width of 1 ms; summed for 100 stimulus trials) using a computer. During constructing PSTHs, the monkey sat quietly without performing any tasks. MI stimulation induced movements of corresponding body parts, but SMA stimulation did not. Only the neurons with apparent cortical inputs were sampled. To confirm the monosynaptic nature of orthodromic excitation, double-cortical stimulation with short intervals (20–50 ms) was applied in some neurons. Then, the neuronal activity during the performance of a goal-directed reaching task with delay was recorded. Timings of neuronal firings and task events (S1, S2, HR, FI, and R) were stored on a computer at a time resolution of 1 ms. These data, along with raw neuronal activity, were also stored on videotapes using a pulse-code modulation recorder (Cygnus Technology, Delaware Water Gap, PA). Finally, the responses of putaminal neurons to somatosensory stimuli, such as passive joint movements and muscle palpations and/or active forelimb movements, were examined.

During daily recording sessions, electromyograms (EMGs) were recorded five times for monkey S and six times for monkey A using surface electrodes from the following muscles: wrist extensor, wrist flexor, biceps brachii, triceps brachii, deltoid, trapezius, upper trunk, lower trunk, and quadriceps femoris. EMG signals were amplified, filtered (100–1,000 Hz), rectified, and stored on a computer.

Data analysis. On the basis of the firing frequency and patterns, putaminal neurons can be classified largely into two groups: phasically active neurons (PANs), which are silent at rest but phasically active during voluntary movements, and tonically active neurons (TANs), which exhibit tonic background discharges at ~2–10 Hz and have longer spike duration than PANs (Alexander and DeLong 1985b; Aosaki et al. 1994; Kimura 1995). The majority of PANs are considered as medium, spiny γ-aminobutyric acid (GABA)ergic-projection neurons, whereas TANs are considered as large, aspiny-cholinergic interneurons (Inokawa et al. 2010). In the present study, PANs, which met the following criteria, were sampled: *1*) firing rate at rest not more than 5 Hz and *2*) spike duration not more than 3 ms.

Responses to cortical stimulation were analyzed by PSTHs (summed for 100 stimulus trials). The mean value and SD of the firing rate during 100 ms, preceding the onset of stimulation, were calculated from PSTHs and were considered to be the value for base discharge (spontaneous firing rate). Responses to the cortical stimuli were judged to be significant if the firing rate during at least three consecutive bins (3 ms) reached the significant level of base discharge + 2 SD ($P = 0.0228$). The latency of the response was defined as the time at which the firing rate first exceeded this level. The responses whose latencies were <21 ms were investigated in this study, as they were mediated by the direct corticostriatal projections based on our previous study (Nambu et al. 2002; see also DISCUSSION).

Neuronal activity during task performance was aligned with the task events (S1, S2, HR, FI, and R) separately, according to the S1 conditions (Left, Center, and Right targets and No-go trials) and shown in raster display. Then, spike-density functions ($\sigma = 13$ ms) were calculated. For detecting delay-related activity, the mean value and SD of the firing rate during 1,000 ms, preceding the S1, were calculated and were considered to be the value for base discharge. Activity changes during the delay periods were judged to be significant if the firing rate reached continuously the significant level of mean discharge + 2 SD ($P = 0.0228$) during at least 3 ms before the S2 (see Anderson and Horak 1985). For detecting movement-related activity, the mean value and SD of the firing rate during 500 ms, preceding the S2, were calculated. Activity changes during the arm-reach movements were judged to be significant if the firing rate reached continuously the significant level of mean discharge + 2 SD ($P = 0.0228$) during at least 3 ms in a 1,200-ms period centered at the HR. The periods of arm-reach movements include the timing of the FI. The latency of the neural response in reference to specific events, such as S1 and HR, was defined as the time at which the firing rate first exceeded this level (mean discharge + 2 SD for 3 ms), aligned with corresponding events. Amplitude (A) of responses related to each event was defined as the averaged number of spikes during the following periods: delay-related activity, a 500-ms period before the S2; HR-related activity, a 1,000-ms period centered at the HR; FI-related activity, a 1,000-ms period centered at the FI. Responses of delay-, HR-, and FI-related activity were modulated by target directions. Directional selectivity of each neuron in each event was defined as: directional selectivity $= 1 - (A_{med} + A_{min})/(A_{max} \times 2)$, where A_{max}, A_{med}, and A_{min} are the maximum, medium, and minimum amplitudes among three targets, respectively ($0 \leq$ directional selectivity ≤ 1; directional selectivity $= 0$ means the same amplitude among three targets). In each neuron, spike-density histograms, showing the largest changes among three targets, were selected. Population activity was calculated by averaging spike-density histograms. The latency of the neuron was defined as the latency of the neural response with the largest changes among three targets.

EMG activity was also analyzed using similar methods. EMG activity during task performance was averaged with the task events separately, according to the S1 conditions. The mean value and SD of the activity during 1,000 ms, preceding the S1, were calculated and were considered to be the values for base activity. EMG activity changes were judged to be significant if the activity reached the significant level of base activity + 2 SD during at least 3 ms. The latency of the EMG activity was defined as the time at which the activity first exceeded this level.

Histology. At the end of the final experiment, several recording sites were marked by passing cathodal direct current (20 μA for 30 s) through the electrode. The monkeys were then anesthetized deeply with sodium pentobarbital (50 mg/kg iv) and perfused transcardially with 2 l of PBS, pH 7.3, followed by 5 l of 8% formalin in 0.1 M phosphate buffer (PB), pH 7.3, and 3 l of 0.1 M PB containing 10% sucrose. The brains were removed, kept in 0.1 M PB containing 30% sucrose at 4°C, and then cut serially into 50 μm-thick frontal sections on a freezing microtome. The sections were mounted onto gelatin-coated glass slides and stained with cresyl violet. The recording sites were reconstructed according to the lesions made by current injection and the traces of electrode tracks. The positions of cortical stimulation electrodes were also confirmed histologically.

RESULTS

EMG activity. Figure 2 shows a typical example of EMG activity during task performance. EMG activity was aligned with HR (Go trials, at *time 0*) or S2 (No-go trials) and averaged separately, according to the S1 conditions. In Go trials, no significant activity changes were observed during the delay period. Large activity increase in forelimb muscles, such as the wrist extensor, wrist flexor, and biceps brachii muscles began preceding the HR. Among them, the biceps brachii muscle displayed the earliest EMG changes, preceding the HR by 170 ms. This activity before the HR may contribute to HR from the resting position. The wrist extensor, biceps brachii, and deltoid muscles showed different activities among Left, Center, and Right target trials, and this may determine the direction of reaching. The wrist flexor and extensor muscles showed large EMG activity 200–600 ms after the HR and may contribute to hand shaping at the final stage of reaching. The upper-trunk muscles were also active during movements, whereas no obvious activity was observed in the lower trunk or hindlimbs. In No-go trials, no significant changes of EMG activity were detected.

Spontaneous firing rates. In the present study, a total of 821 putaminal neurons, which were classified as PANs, was sampled in two monkeys. Among them, 447 neurons displayed significant excitatory responses to cortical stimulation based on offline analysis and were studied further. The second stimulation of the double-cortical stimulation evoked comparable excitatory responses with those evoked by the first stimulation (data not shown), suggesting that the excitatory responses were mediated by direct corticostriatal projections. According to the cortical inputs, putaminal neurons were classified into three groups: MI-, SMA-, and MI + SMA-recipient neurons (Nambu et al. 2002). MI-recipient neurons were further classified into $MI_{proximal}$-, MI_{distal}-, and $MI_{proximal + distal}$-recipient neurons. MI + SMA-recipient neurons were also classified into $MI_{proximal}$ + SMA-, MI_{distal} + SMA-, and $MI_{proximal + distal}$ + SMA-recipient neurons. The number of neurons belonging to each group and their spontaneous firing rates are shown in Table 1. A considerable number of neurons received convergent inputs from multiple cortical areas. The spontaneous firing rate of MI-recipient neurons [1.41 ± 1.82 (SD) Hz] was significantly lower than those of SMA (2.50 ± 2.67

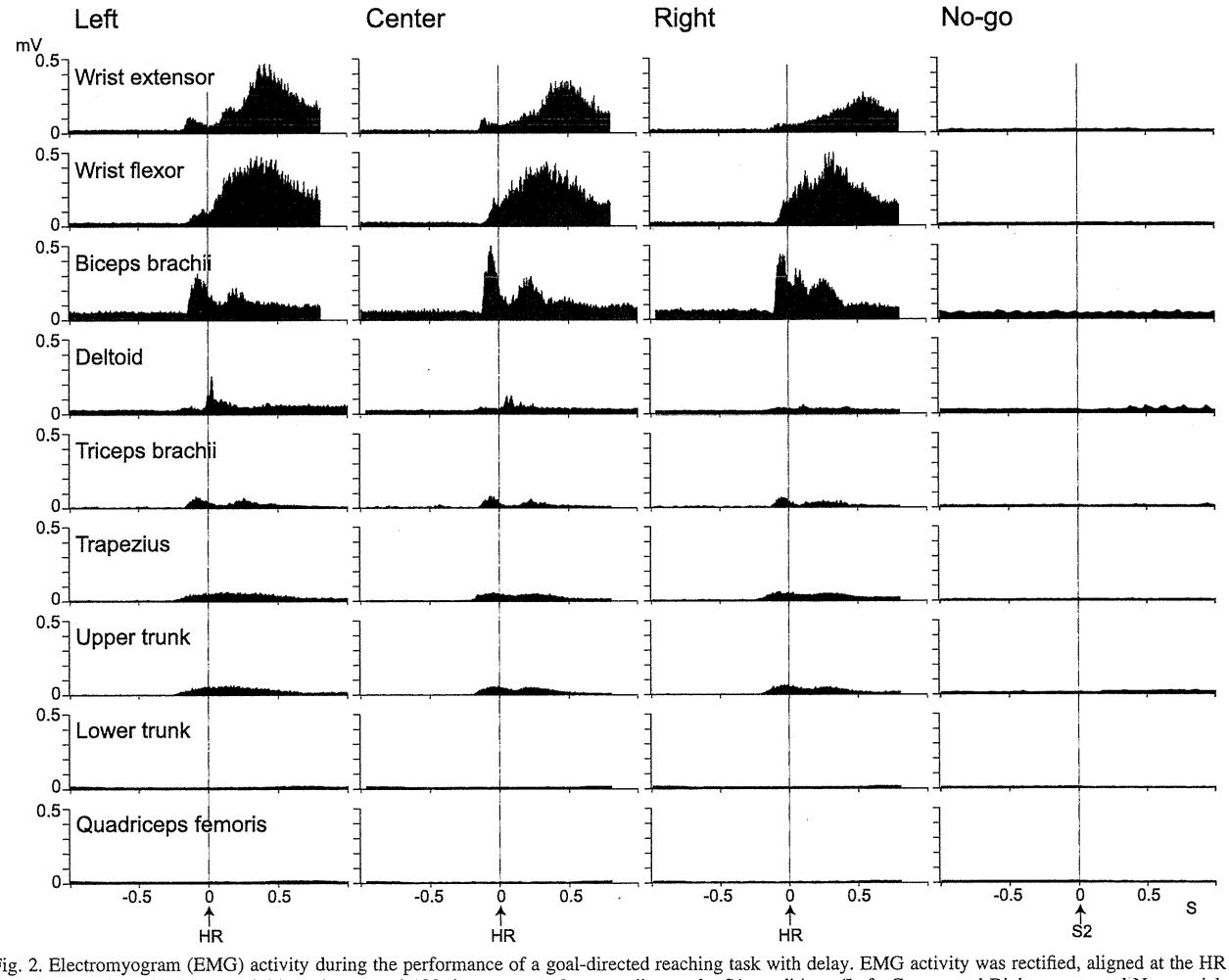

Fig. 2. Electromyogram (EMG) activity during the performance of a goal-directed reaching task with delay. EMG activity was rectified, aligned at the HR (Go trials, at *time 0*) or S2 (No-go trials), and averaged 100 times separately, according to the S1 conditions (Left, Center, and Right targets and No-go trials). In Go trials, EMG activity was observed in the forelimb and upper-trunk muscles but not in the lower-trunk and hindlimb muscles. No EMG activity was observed in No-go trials.

Table 1. *Classification of putaminal neurons and their spontaneous firing rates*

Cortical inputs	Number of neurons			Spontaneous firing rate
	Monkey S	Monkey A	Total	(mean ± SD, Hz)
MI			246 (55)	1.41 ± 1.82*,†
$MI_{proximal}$	40	76	116 (26)	1.34 ± 1.70
MI_{distal}	26	40	66 (15)	1.40 ± 1.99
$MI_{proximal + distal}$	21	43	64 (14)	1.77 ± 1.84
SMA	50	60	110 (25)	2.50 ± 2.67*
MI + SMA			91 (20)	2.48 ± 2.20†
$MI_{proximal}$ + SMA	20	26	46 (10)	2.18 ± 1.86
MI_{distal} + SMA	8	20	28 (6)	2.18 ± 2.51
$MI_{proximal + distal}$ + SMA	5	12	17 (4)	3.66 ± 2.24
Total	170	277	447 (100%)	1.90 ± 2.17

Numbers of putaminal neurons in two monkeys and their spontaneous firing rates are shown according to cortical inputs. Figures in parentheses indicate the percentage to the total number of neurons. Spontaneous firing rates were calculated from peristimulus time histograms during 100 ms preceding the onset of cortical stimulation without any behavioral tasks (see MATERIALS AND METHODS). MI_{distal} and $MI_{proximal}$, distal and proximal forelimb regions of the primary motor cortex, respectively; SMA, forelimb region of the supplementary motor area. *,†Significantly different from each other (Bonferroni/Dunn post hoc tests; $P < 0.05$).

Hz)- and MI + SMA (2.48 ± 2.20 Hz)-recipient neurons ($P < 0.05$; Bonferroni/Dunn post hoc tests).

The latencies of excitations in putaminal neurons evoked by each cortical stimulation are compared in Fig. 3. The latency of $MI_{proximal}$-induced excitation (10.9 ± 2.5 ms; Fig. 3*A*) and that of MI_{distal}-induced excitation (11.5 ± 2.6 ms; Fig. 3*B*) was significantly shorter than that of SMA-induced excitation (14.1 ± 2.8 ms; Fig. 3*C*; Bonferroni/Dunn post hoc tests; $P < 0.05$). The latencies of the excitation evoked by stimulation

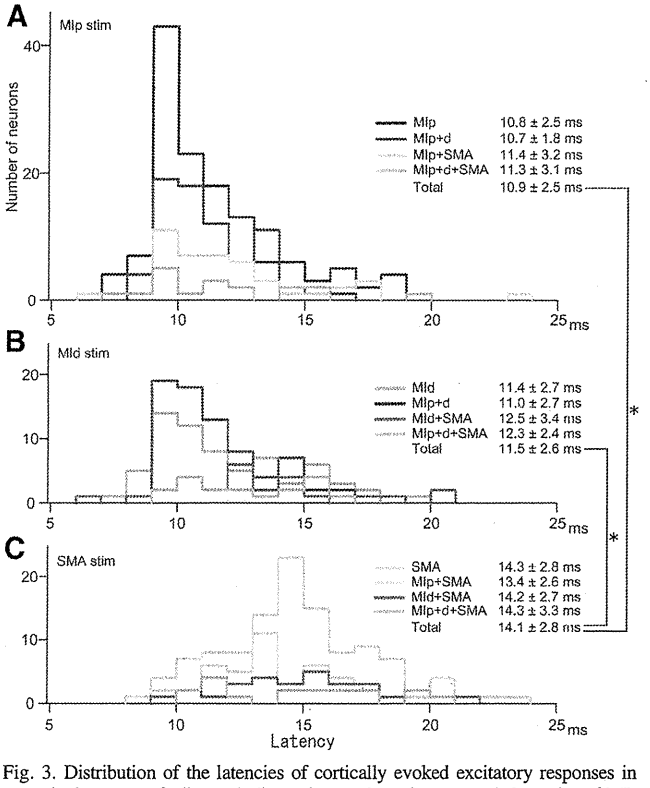

Fig. 3. Distribution of the latencies of cortically evoked excitatory responses in putaminal neurons. Ordinates indicate the number of neurons. *A*: latencies of MI- and MI + SMA-recipient neurons to $MI_{proximal}$ stimulation. *B*: latencies of MI- and MI + SMA-recipient neurons to MI_{distal} stimulation. *C*: latencies of SMA- and MI + SMA-recipient neurons to SMA stimulation. *Significantly different from each other (Bonferroni/Dunn post hoc tests; $P < 0.05$).

in the same cortical area were comparable between neurons with converging inputs and neurons with a single cortical input (Fig. 3).

Activity during task performance. Activity of putaminal neurons with different cortical inputs is exemplified in Figs. 4–6. Figure 4*A* shows a typical example of $MI_{proximal}$-recipient putaminal neurons. This neuron received cortical input exclusively from the $MI_{proximal}$. $MI_{proximal}$ stimulation evoked excitatory responses at a latency of 11 ms (Fig. 4*A1*), whereas stimulation of other cortical areas did not. Neuronal activity during task performance was aligned with the S1 and HR (Go trials) or the S1 and S2 (No-go trials) separately, according to the S1 conditions, and averaged (Fig. 4*A2*). This neuron exhibited no activity during the delay period and increased activity in relation to arm-reach movements, preceding the HR by 125 ms. The amplitude of movement-related activity was larger in the Right target trials than in the Center and Left target trials. Directional selectivity of the HR-related activity was 0.60. No activity was observed in No-go trials. Somatosensory examination revealed that this neuron was activated by lateral rotation of the shoulder. These observations suggest that this neuron increased activity in relation to the proximal forelimb movement, such as HR from the resting position.

Figure 4*B* shows a typical example of MI_{distal}-recipient putaminal neurons. This neuron received cortical input exclusively from the MI_{distal}. MI_{distal} stimulation evoked excitatory responses at a latency of 15 ms (Fig. 4*B1*), whereas stimulation of other cortical areas did not. This neuron exhibited no activity during the delay period (Fig. 4*B2*). This neuron showed a mild activity increase after the HR in the Right target trials and a large activity increase around the FI in all three targets conditions. The timing-of-activity increase correlated with the FI, not with the S2, HR, or R. No activity was observed in No-go trials. Directional selectivity of the FI-related activity was 0.21. This neuron was activated by abduction of the wrist. These observations suggest that this neuron increased activity in relation to the distal forelimb movement, such as shaping its hand for touching the target slot.

Figure 5, *A* and *B*, shows two examples of SMA-recipient putaminal neurons. These neurons received cortical input exclusively from the SMA. The neuron in Fig. 5*A* responded

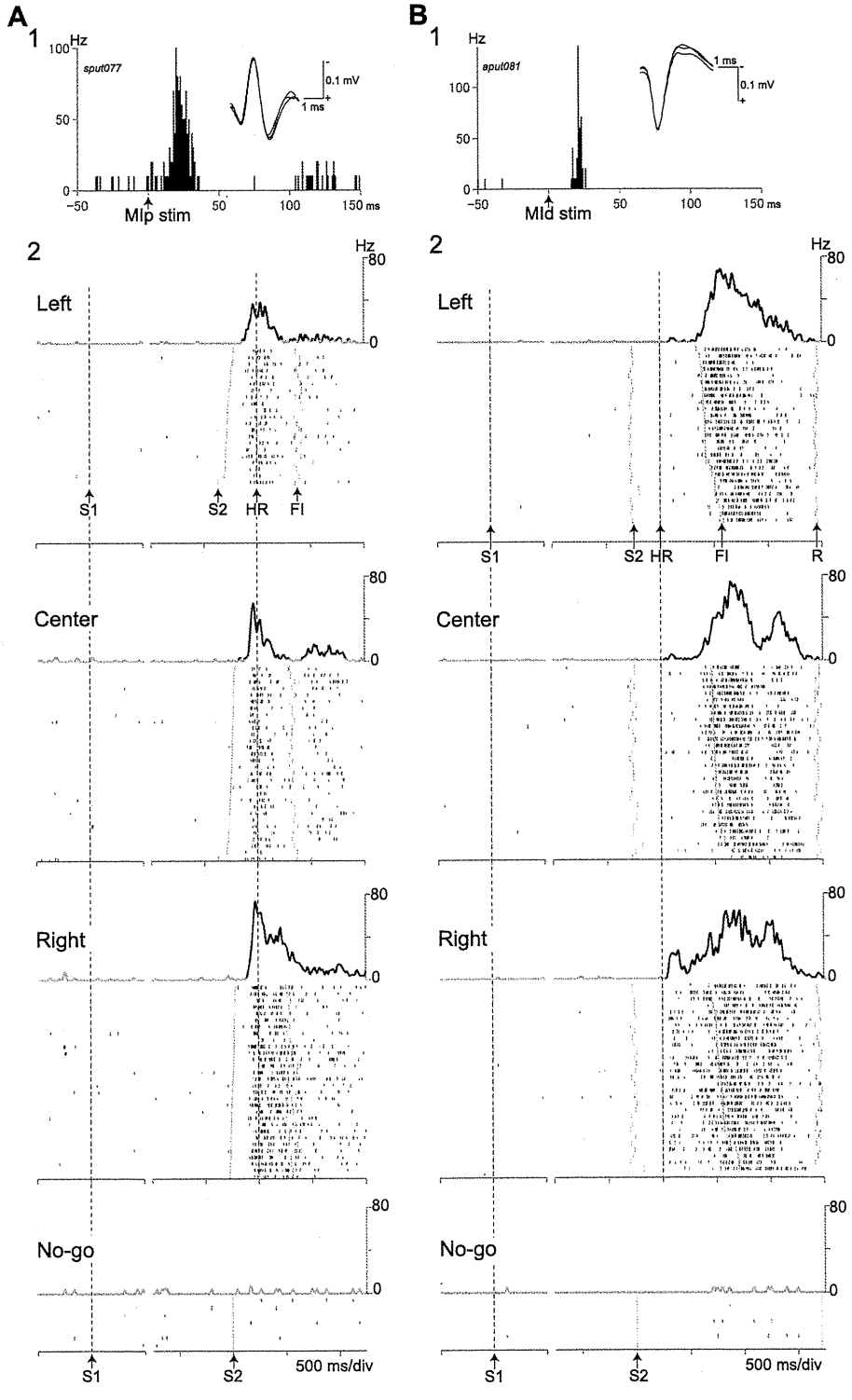

Fig. 4. *A*: typical example of $MI_{proximal}$-recipient putaminal neurons. *A1*: peristimulus time histograms (PSTHs; bin width of 1 ms; 100 stimulus trials) showing responses to $MI_{proximal}$ stimulation (duration 300 μs, single pulse, 0.4 mA). Voltage traces of action potentials are shown as an inset. *A2*: raster display showing the neuronal firing (short, black vertical lines) during the performance of a goal-directed reaching task with delay. Neuronal activity was aligned separately according to the S1 conditions (Left, Center, and Right targets and No-go trials, from *top* to *bottom*) with the S1 (*left*), and HR (*right*; in Go trials) or S2 (*right*; in No-go trials). Short, gray vertical lines indicate the timing of the S2 and FI. Each plot of Go trials was sorted according to the reaction time (S2-HR). Continuous, gray traces indicate spike-density functions (σ = 13 ms) for the associated rasters. For the spike-density functions in this and the following figures, the mean value and SD of the firing rate during 1,000 ms, preceding the S1, were calculated. The spike-density functions with significant changes, which continuously reach the significant level of mean discharge + 2 SD during at least 3 ms, are indicated by black traces. Abscissa, ticked every 500 ms. *B*: typical example of MI_{distal}-recipient putaminal neurons. *B1*: PSTHs showing responses to MI_{distal} stimulation (0.4 mA). *B2*: raster display showing the neuronal firing during task performance. Each plot of Go trials was sorted according to the movement time (HR-FI). The timing of the R is also indicated by short, gray vertical lines.

to SMA stimulation at a latency of 12 ms (Fig. 5*A1*), whereas stimulation of other cortical areas did not. This neuron showed delay-related activity, i.e., a gradual firing-rate increase beginning after the S1 and lasting before S2 (Fig. 5*A2*). Delay-related activity was observed in all three target conditions, and directional selectivity of delay-related activity was 0.21. The activity increased additionally and reached its peak after the HR, suggesting that this neuron also showed movement-related activity. Although the activity increase was also observed in No-go trials, its amplitude was smaller than that in Go trials. This neuron was activated during active shoulder movements. Figure 5*B* shows another

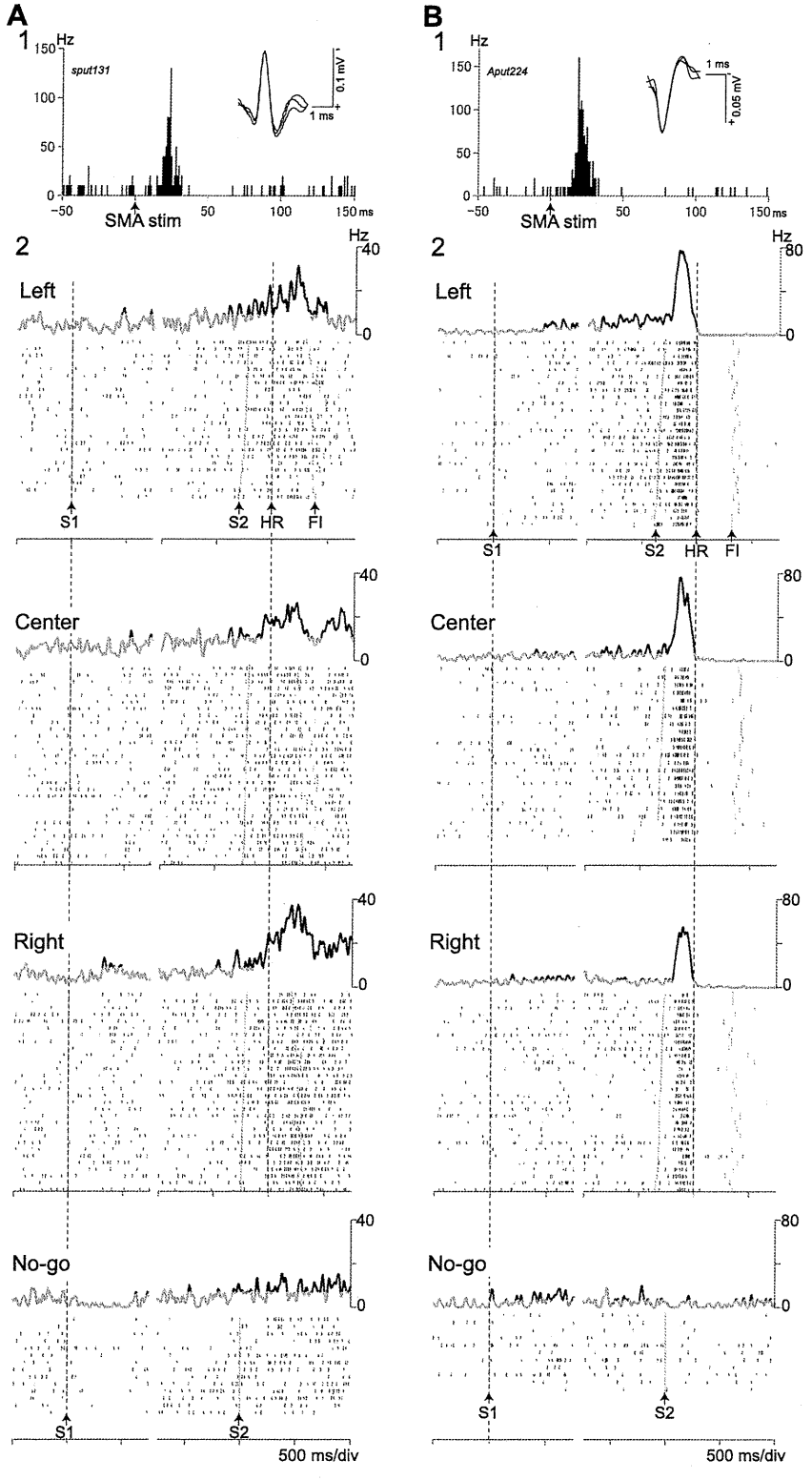

Fig. 5. Two examples (*A* and *B*) of SMA-recipient putaminal neurons. *A1* and *B1*: PSTHs showing responses to SMA stimulation (0.6 mA). *A2* and *B2*: raster display showing the neuronal firing during task performance.

example of SMA-recipient putaminal neurons. This neuron responded to SMA stimulation at a latency of 10 ms (Fig. 5*B1*), whereas stimulation of other cortical areas did not. This neuron exhibited a delay-related activity (directional selectivity, 0.22) and a large movement-related activity increase preceding the HR by 252 ms (Fig. 5*B2*). Directional selectivity of the HR-related activity was 0.38. This neuron was activated by passive shoulder movements.

Figure 6*A* shows a typical example of $MI_{proximal}$ + SMA-recipient putaminal neurons. This neuron received

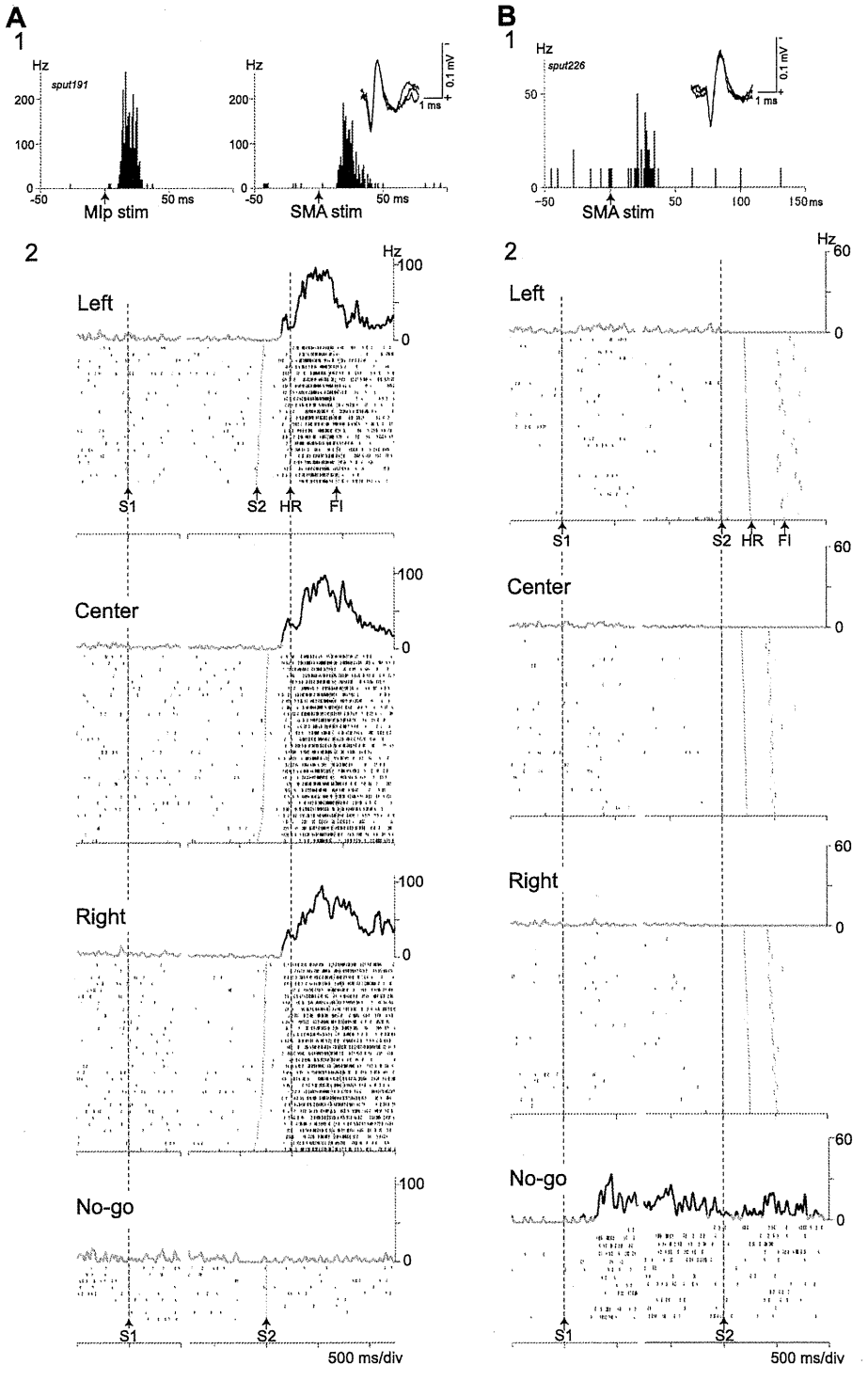

Fig. 6. *A*: typical example of $MI_{proximal}$ + SMA-recipient putaminal neurons. *A1*: PSTHs showing responses to $MI_{proximal}$ stimulation (0.6 mA, *left*) and SMA stimulation (0.5 mA, *right*). *A2*: raster display showing the neuronal firing during task performance. *B*: No-go-specific activity. *B1*: PSTHs showing responses to SMA stimulation (0.6 mA). *B2*: raster display showing the neuronal firing during task performance.

convergent cortical inputs from the $MI_{proximal}$ and SMA. $MI_{proximal}$ and SMA stimulation evoked excitatory responses at latencies of 9 ms and 14 ms, respectively (Fig. 6*A1*), whereas MI_{distal} stimulation did not. This neuron increased activity in relation to arm-reach movements, preceding the HR by 106 ms (Fig. 6*A2*). The amplitude of excitation was comparable among the three target conditions. Directional selectivity of the HR-related activity was 0.15. No activity was observed in No-go trials. This neuron was activated by extension and abduction of the shoulder.

Among 447 putaminal neurons recorded, most neurons (412/447, 92.2%) exhibited activity increases in Go trials and almost no activity in No-go trials. Twenty-two neurons (4.9%) showed no significant activity changes in either Go or No-go trials. Six neurons (1.3%) showed a comparable activity increase in both Go and No-go trials and were classified as MI + SMA-

Table 2. *Activity patterns of putaminal neurons during task performance*

Cortical inputs	Delay-related	Movement-related	Total
MI	39 (16)*	213 (87)†,‡	246
$MI_{proximal}$	23 (20)	107 (92)	116
MI_{distal}	11 (17)	55 (83)	66
$MI_{proximal + distal}$	5 (8)	51 (80)	64
SMA	35 (32)*	78 (71)†	110
MI + SMA	21 (23)	65 (71)‡	91
$MI_{proximal}$ + SMA	13 (28)	32 (70)	46
MI_{distal} + SMA	5 (18)	21 (75)	28
$MI_{proximal + distal}$ + SMA	3 (18)	12 (71)	17
Total	95 (21)	356 (80)	447

Numbers of putaminal neurons showing delay-related and/or movement-related activity are shown according to cortical inputs. Figures in parentheses indicate the percentage to each category of neurons. *,†,‡Significantly different from each other (χ^2 test with Bonferroni correction; $P < 0.05$). Note that some neurons showed both delay- and movement-related activity.

recipient neurons. Seven neurons (1.6%) showed an activity increase in No-go trials and no activity in Go trials (No-go-specific activity), as exemplified in Fig. 6*B*, and were classified as SMA-recipient neurons. SMA stimulation evoked excitatory responses at a latency of 20 ms (Fig. 6*B1*). This neuron increased activity at 395 ms after the S1, maintained activity, and decreased activity before the Reward in No-go trials (Fig. 6*B2*), whereas no activity in Go trials. This neuron was not activated either by passive body movements or by visual stimuli.

Putaminal neurons with different cortical inputs showed different activity patterns during task performance (Table 2). The activity patterns of MI-recipient neurons are significantly different from those of SMA- and MI + SMA-recipient neurons (χ^2 test with Bonferroni correction, $P < 0.05$). Most of MI-recipient neurons (87%) showed movement-related activity, whereas some neurons (16%) showed delay-related activity. More SMA-recipient neurons (32%) showed delay-related activity than MI-recipient neurons, and fewer ones (71%) showed movement-related activity. MI + SMA-recipient neurons showed activity patterns intermediate between MI- and SMA-recipient neurons. The ratio of MI + SMA-recipient neurons showing delay-related activity was smaller than that of SMA-recipient neurons, and the ratio of MI + SMA-recipient neurons showing movement-related activity was smaller than that of MI-recipient neurons.

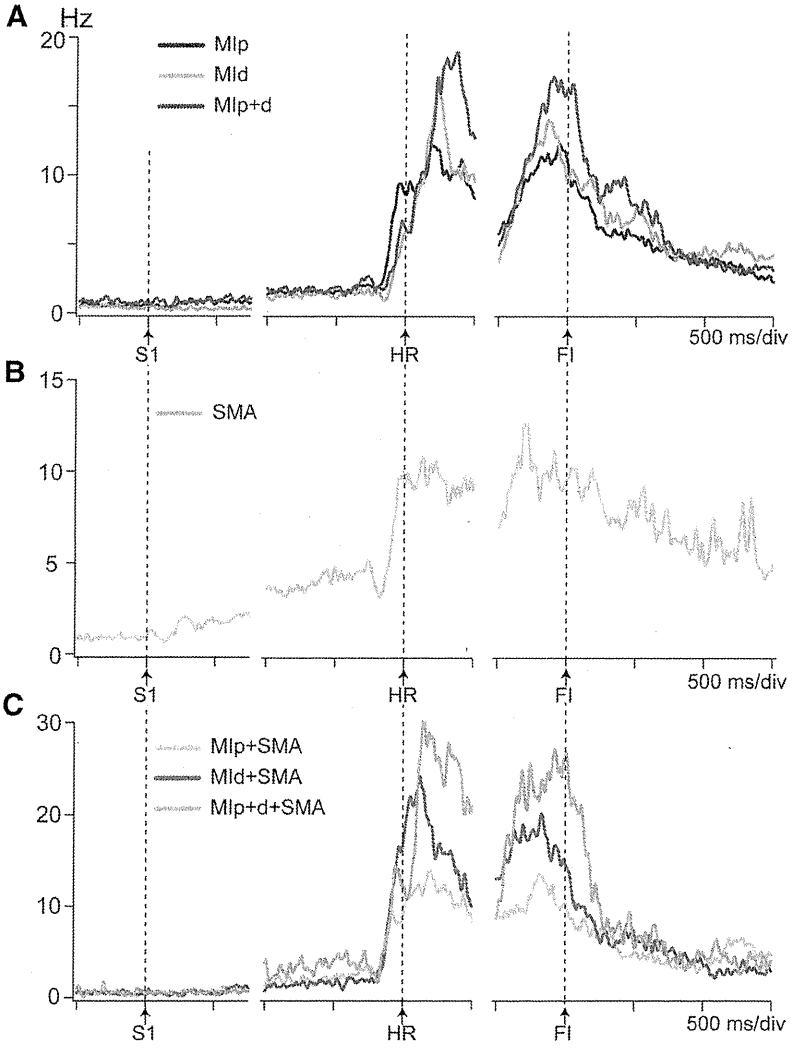

Fig. 7. Population activity of putaminal neurons during task performance. *A*: population activity of $MI_{proximal}$-, MI_{distal}-, and $MI_{proximal + distal}$-recipient putaminal neurons (shown in different colors) aligned with the S1 (*left*), HR (*middle*), and FI (*right*). *B*: population activity of SMA-recipient putaminal neurons. *C*: population activity of $MI_{proximal}$ + SMA-, MI_{distal} + SMA-, and $MI_{proximal + distal}$ + SMA-recipient putaminal neurons (shown in different colors).

Characteristics of putaminal neuronal activity during task performance were also observed in population activity (Fig. 7). MI-recipient neurons showed very little changes during the delay period (Fig. 7*A*). The firing rate increased abruptly before the HR, preceding the HR by 154 ms in $MI_{proximal}$-recipient neurons, by 119 ms in MI_{distal}-recipient neurons and by 123 ms in $MI_{proximal\ +\ distal}$-recipient neurons. Activity increase reached its peak before the FI. SMA-recipient neurons showed a gradual activity increase during the delay period, beginning 197 ms after the S1 (Fig. 7*B*). They showed additional activity increase in relation to arm-reach movements, preceding the HR by 303 ms. MI + SMA-recipient neurons also showed a gradual activity increase during the delay period (Fig. 7*C*). They showed additional activity increase in relation to arm-reach movements, preceding the HR by 134–138 ms ($MI_{proximal}$ + SMA-, 135 ms; MI_{distal} + SMA-, 138 ms; $MI_{proximal\ +\ distal}$ +SMA-, 134 ms).

Timing of activity changes of putaminal neurons. The onset timing of movement-related activity changes in relation to the HR was shown in cumulative distributions (Fig. 8). Very early activity changes that preceded the HR by more than 400 ms in SMA-recipient neurons were considered to reflect activity during the delay period. Approximately one-half of $MI_{proximal}$ (47%)-, SMA (49%)-, $MI_{proximal}$ + SMA (57%)-, M_{distal} + SMA (44%)-, and $MI_{proximal\ +\ distal}$ + SMA (54%)-recipient neurons changed activities before the HR, whereas a smaller number of MI_{distal} (28%)- and $MI_{proximal\ +\ distal}$ (40%)-recipient neurons did. The earliest EMG changes began 170 ms before the HR (Fig. 3). In some of $MI_{proximal}$ (9%)-, MI_{distal} (7%)-, $MI_{proximal\ +\ distal}$ (9%)-, SMA (21%)-, $MI_{proximal}$ + SMA (17%)-, MI_{distal} + SMA (5%)-, and $MI_{proximal\ +\ distal}$ + SMA (15%)-recipient neurons, their activity changes preceded the earliest EMG changes.

The onset latencies of delay-related activity after the S1 were comparable among MI (502 ± 47 ms)-, SMA (469 ± 47 ms)-, and MI + SMA (471 ± 96 ms)-recipient neurons.

Direction selectivity. The amplitude of activity during task performance was modulated by the target direction. Directional selectivity of delay-, HR-, and FI-related activity was calculated in each neuron group (Table 3 and Fig. 9). Concerning HR-related activity, MI-recipient putaminal neurons showed significantly higher directional selectivity than SMA- and MI + SMA-recipient neurons (Bonferroni/Dunn post hoc tests; $P < 0.05$). Among them, $MI_{proximal}$-recipient putaminal neurons showed the highest directional selectivity. One-third of $MI_{proximal}$-recipient neurons (32%) had directional selectivity ≥0.5, whereas a smaller number of other neuron groups did (Fig. 9). Concerning FI-related activity, MI-recipient putaminal neurons showed significantly higher directional selectivity than MI + SMA-recipient neurons ($P < 0.05$). Directional selectivity of delay-related activity was comparable among MI-, SMA-, and MI + SMA-recipient putaminal neurons.

Locations of recorded putaminal neurons. The locations of putaminal neurons recorded were plotted in frontal sections (Fig. 10). The neurons that responded to stimulation of the forelimb regions of the MI and/or SMA were distributed in a band extending from the ventrolateral to dorsomedial part in the caudal aspect of the putamen. Within this band, MI-recipient neurons were located mainly in the ventral part, whereas SMA-recipient neurons were found in the dorsal part. MI + SMA-recipient neurons were located in between. In

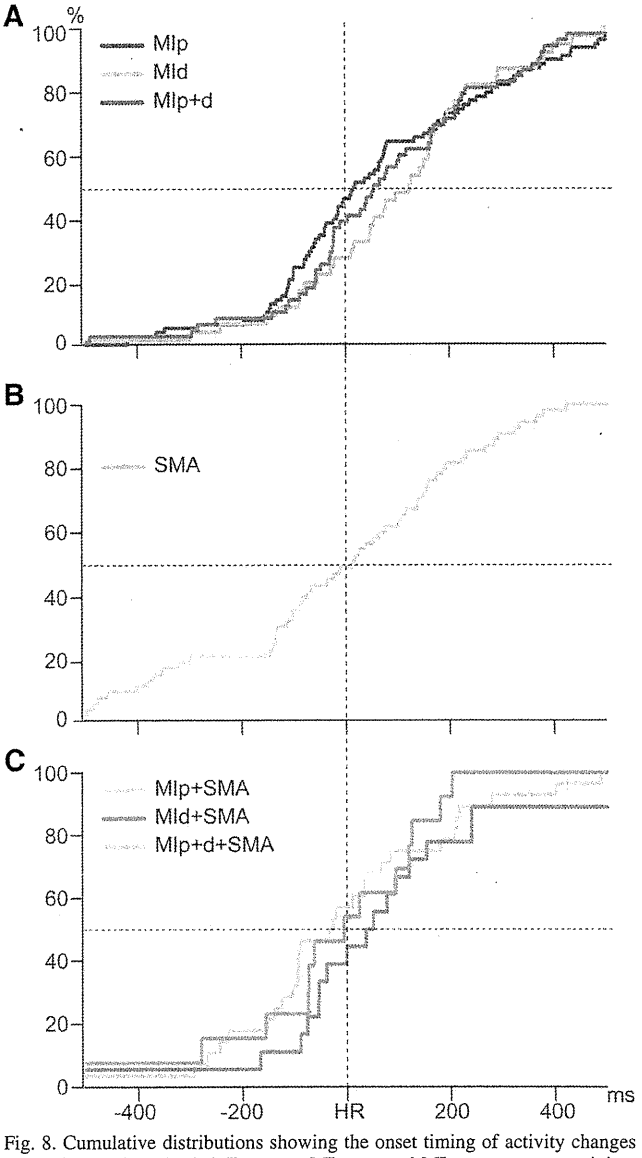

Fig. 8. Cumulative distributions showing the onset timing of activity changes in relation to the HR. *A*: $MI_{proximal}$-, MI_{distal}-, and $MI_{proximal\ +\ distal}$-recipient putaminal neurons (shown in different colors). *B*: SMA-recipient putaminal neurons. *C*: $MI_{proximal}$ + SMA-, MI_{distal} + SMA-, and $MI_{proximal\ +\ distal}$ + SMA-recipient putaminal neurons (shown in different colors).

MI-recipient neurons, MI_{distal}- and $MI_{proximal\ +\ distal}$-recipient neurons were situated predominantly in the ventral-most part. MI- and SMA-recipient neurons showed different activity patterns during task performance (Table 2). Thus neurons in the ventrolateral part of the putamen receive inputs from the MI and show movement-related activity, whereas neurons in the dorsomedial part receive inputs from the SMA and show both movement- and delay-related activity.

The neurons that did not show task-related activity were distributed randomly in the MI- and SMA-recipient band (Fig. 10). The neurons that did not respond to the MI and SMA stimulation were distributed dorsolaterally or ventromedially to the band. Putaminal neurons situated dorsally to the MI-recipient zone often responded to manipulation of the hip joint, and microstimulation in this area evoked movements of the hip

Table 3. *Directional selectivity of putaminal neurons*

Cortical inputs	Directional selectivity (mean ± SD)		
	Delay-related	HR-related	FI-related
MI	0.27 ± 0.18	0.39 ± 0.21*,†	0.37 ± 0.20‡
$MI_{proximal}$	0.23 ± 0.14	0.41 ± 0.23	0.39 ± 0.20
MI_{distal}	0.34 ± 0.25	0.33 ± 0.18	0.33 ± 0.20
$MI_{proximal + distal}$	0.29 ± 0.15	0.37 ± 0.17	0.38 ± 0.20
SMA	0.31 ± 0.19	0.33 ± 0.19*	0.35 ± 0.19
MI + SMA	0.22 ± 0.12	0.31 ± 0.19†	0.29 ± 0.17‡
$MI_{proximal}$ + SMA	0.18 ± 0.09	0.31 ± 0.19	0.32 ± 0.18
MI_{distal} + SMA	0.36 ± 0.12	0.38 ± 0.17	0.29 ± 0.15
$MI_{proximal + distal}$ + SMA	0.16 ± 0.06	0.17 ± 0.11	0.18 ± 0.11

Directional selectivity of Delay-related, Hand Release (HR)-related, and Finger In (FI)-related activity is shown according to cortical inputs. *,†,‡Significantly different from each other (Bonferroni/Dunn post hoc tests; $P < 0.05$).

joint. In contrast, putaminal neurons situated ventrally to the MI-recipient zone responded to manipulation of the orofacial region, and microstimulation in this area evoked orofacial movements. Neurons in the orofacial areas of the putamen increased activity in relation to orofacial movements, such as licking juice at reward periods.

DISCUSSION

The present study revealed the following results. *1*) Putaminal neurons with inputs from different cortical areas showed distinct activity patterns during the performance of a goal-directed reaching task with delay. *2*) MI-recipient neurons increased activity in response to arm-reach movements, whereas SMA-recipient neurons increased activity during delay periods as well as during movements. The activity pattern of MI + SMA-recipient neurons was of an intermediate type between those of MI- and SMA-recipient neurons. *3*) Approximately one-half of $MI_{proximal}$-, SMA-, and MI + SMA-recipient neurons changed activities before the onset of movements, whereas a smaller number of MI_{distal}- and $MI_{proximal + distal}$-recipient neurons did. *4*) MI-recipient neurons showed higher directional selectivity during arm-reach movements than SMA- and MI + SMA-recipient neurons. *5*) MI-recipient neurons were located mainly in the ventrolateral part of the caudal aspect of the putamen, whereas SMA-recipient neurons were located in the dorsomedial part. MI + SMA-recipient neurons were found in between.

Methodological considerations. Electrophysiological recording at the distance of 2.5 mm from the electrode implantation sites showed no excitation of cortical neurons after stimulation (up to 0.7 mA) in our previous work (Nambu et al. 2002). Therefore, the extent of the current spread from stimulating electrodes implanted in the cortex was estimated to be <2.5 mm. $MI_{proximal}$ and MI_{distal} electrode implantation sites were 2.5–3.2 mm apart (Fig. 1*B*), and stimulation in the $MI_{proximal}$ and MI_{distal} evoked movements in the proximal and distal forelimb regions, respectively, in the present study. Thus stimulation in the $MI_{proximal}$, MI_{distal}, and SMA is considered to have excited each cortical area specifically.

The orthodromic responses evoked by cortical stimulation in the present study are considered to be mediated by direct corticostriatal projections as discussed below. The excitatory responses followed well the double-cortical stimulation with short intervals (20–50 ms), suggesting that they are monosynaptic responses. The distribution of the orthodromically activated putaminal neurons corresponds well to that of $MI_{proximal}$-, MI_{distal}-, and SMA-derived corticostriatal terminals reported previously (Künzle 1975; Liles and Updyke 1985; Takada et al. 1998a, b; Tokuno et al. 1999). The latency of MI-evoked orthodromic responses of putaminal neurons in this study was within the same range as that of corticostriatal-evoked responses in the monkey (Liles 1975; Nambu et al. 2002) and putamen-evoked antidromic activation of MI neurons (Bauswein et al. 1989; Turner and DeLong 2000).

MI + SMA-recipient putaminal neurons in the present study are considered to receive converging inputs directly from the MI and SMA. It might be argued that excitatory responses in MI + SMA-recipient putaminal neurons evoked by SMA stimulation could be mediated by the SMA-MI and MI-putamen projection but not by the direct SMA-putamen projection. If this were the case, the neurons in the center of the MI-recipient putaminal zone might also be expected to respond to SMA stimulation. However, the MI + SMA-recipient putaminal neurons were located only in the intermediate zone between the laterally situated MI-recipient and medially situated SMA-recipient zones (Fig. 10), corresponding well to the distribution patterns of corticostriatal terminals from these cortical areas (Takada et al. 1998a, b). The fact that the latency of MI + SMA-recipient putaminal neurons to SMA stimulation was similar to that of SMA-recipient putaminal neurons to SMA stimulation (Fig. 3) also supports the argument that SMA stimulation does not activate MI + SMA-recipient putaminal neurons indirectly.

Another issue is whether MI and SMA stimulation can excite entire forelimb regions of the MI and SMA, respectively. Two pairs of bipolar-stimulating electrodes in the MI cover large areas of the forelimb region of the MI (Fig. 1*B*). A pair of bipolar-stimulating electrodes in the SMA covers most of the forelimb region of the SMA. MI- and SMA-recipient zones studied by orthodromic responses evoked by cortical stimulation correspond well to the zones examined by somatosensory inputs, movements evoked by intrastriatal microstimulation (Nambu et al. 2002), and corticostriatal terminals (Takada et al. 1998a, b). Outside of the MI- and SMA-recipient zones, putaminal neurons responded to manipulation of the hip joint or the oral region. These results suggest that cortical stimulation successfully covers the forelimb regions of the MI and SMA.

Information processing through the corticostriatal projections. On the basis of previous anatomical (Takada et al. 1998a, b; Tokuno et al. 1999) and electrophysiological (Nambu et al. 2002) studies, the forelimb region of the MI projects mainly to

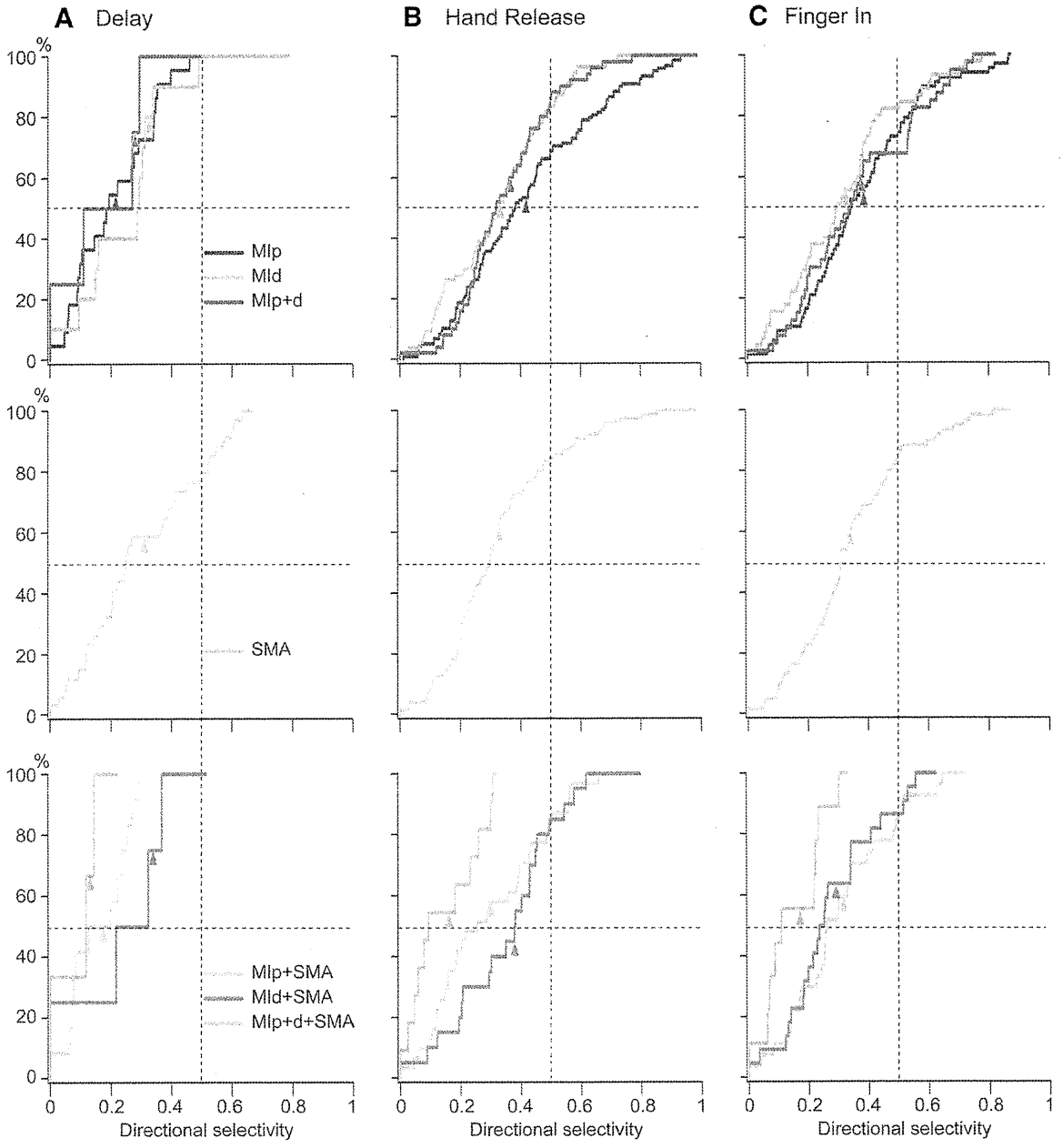

Fig. 9. Cumulative distributions showing the directional selectivity of delay (*A*)-, HR (*B*)-, and FI (*C*)-related activity of $MI_{proximal}$-, MI_{distal}-, and $MI_{proximal + distal}$ (*top row*)-, SMA (*middle row*)-, and $MI_{proximal}$ + SMA-, MI_{distal} + SMA-, and $MI_{proximal + distal}$ + SMA (*bottom row*)-recipient putaminal neurons. Small arrowheads indicate mean.

the lateral part of the caudal aspect of the putamen, whereas that of the SMA projects predominantly to its medial counterpart. In addition, a substantial number of neurons in the mediolateral central zone of the putamen receive convergent inputs from both the MI and SMA (Nambu et al. 2002; Takada et al. 1998a, b). Within the MI- and MI + SMA-recipient zones of the putamen, input from the MI_{distal} enters more ventrally than that from the $MI_{proximal}$ (Nambu et al. 2002; Tokuno et al. 1999). These distributions agree with the present results (Fig. 10). The latency of responses evoked by cortical stimulation was comparable with the previously reported one (Nambu et al. 2002).

The present study has shown that neuronal activity in the putamen is dominated by its cortical inputs. Moreover, a variety of task-related information from different cortical areas might converge onto single putaminal neurons. Many MI-recipient neurons exhibited movement-related activity, whereas SMA-recipient neurons displayed delay-related activity, as well as movement-related activity. The activity onset of the SMA-recipient neurons preceded that of MI-recipient neurons. In addition, some of the SMA-recipient neurons showed No-go-specific activity (Fig. 6*B*). The spontaneous firing rate of MI-recipient neurons was lower than that of the SMA-recipient neurons (Table 1). Such activity patterns of putaminal neurons seem to reflect activities of MI and